Foraminiferal $\delta^{18}O$ reveals gas hydrate dissociation in Arctic and North Atlantic oceans sediments

Pierre-Antoine Dessandier[1*], Giuliana Panieri[1], Chiara Borrelli[1,2], Haoyi Yao[1], Simone Sauer[1,3], Wei-Li Hong[1,4].

[1]CAGE – Centre for Arctic Gas Hydrate, Environment and Climate, Department of Geosciences, UiT The Arctic University of Norway in Tromsø, Norway
[2]University of Rochester, Department of Earth and Environmental Sciences, Rochester, NY, USA.
[3]IFREMER - Institut Français de Recherche pour l'Exploitation de la Mer, Plouzané, France
[4]Geological Survey of Norway, Trondheim, Norway
*Corresponding author: pierre-antoine.dessandier@uit.no

Abstract

Paleoceanographic investigations in the Arctic and north Atlantic are crucial to understanding past and current climate change, in particular considering amounts of pressure-temperature sensitive gas stored in marine sediments of the region. Many paleoceanographic studies are based on foraminiferal oxygen and carbon stable isotope compositions ($\delta^{18}O$, $\delta^{13}C$) from either planktonic specimens, benthic specimens or both. However, in seafloor regions promixal to high upward methane fluxes, such as where seafloor gas emission and shallow gas hydrate-bearing sediment occur, foraminiferal $\delta^{18}O$ and $\delta^{13}C$ display a wide range of values. Our study focuses on foraminiferal stable isotope signatures in shallow sediment at core sites in the Arctic affected by significant upward flow of methane. This includes cores with shallow sulfate methane transitions that are adjacent to seeps and containing gas hydrate. We place emphasis on potential effects due to gas hydrate dissociation and diagenesis. Gas hydrate dissociation is known to increase pore-water $\delta^{18}O$, but our results indicate that precipitation of methane-derived authigenic carbonate (MDAC) also affects the foraminiferal $\delta^{18}O$ of both planktonic and benthic species. In addition to this post-depositional overprint, we investigate the potential bias of the stable isotope record due to ontogenetic effects. Our data show that the size fraction does not impact the isotopic signal of planktonic and benthic foraminifera.

Keywords: Foraminiferal stable isotopes, Arctic Ocean, gas hydrates, authigenic carbonates

1. Introduction

The Arctic is particulary sensitive to climate change (e.g., IPCC13; Screen and Simmonds, 2010; Serreze and Barry, 2011) and mulltiple oceanographic parameters are rapidily changing (Jakobsson et al., 2008). The Arctic is a fundamental component of the climate system because of its role in global carbon cycling (e.g., McGuire et al., 2009). First, the Arctic Ocean sequesters carbon dioxide that enters North Atlantic Deep Water. Second, the Arctic modulates carbon exchange with the atmosphere because of seasonal sea-ice coverage (e.g., McGuire et al., 2009). Third, the region contains very large amounts of methane in permafrost and gas hydrates, both which are sensitive to temperature change (Corell et al., 2008).

Along the Arctic continental shelves and slopes, probably between 30 and 170 Pg of methane exists as gas hydrate (e.g., Kvendvolden 1988; McGuire et al., 2009; James et al., 2016). Gas hydrates are crystalline solids that consist of gas (mostly methane) trapped in a lattice of hydrogen-bonded water molecules (Sloan and Koh, 2007). Hydrates are stable at relatively low (< 10°C) temperatures and moderate (>3-5 MPa) pressures, which at high latitudes generally correspond to water depths greater than 300 m (James et al., 2016). However, warming of intermediate- and deep-water masses or depressurization because of isostatic rebound might trigger hydrate dissociation (Thomas et al., 2002; Yao et al., 2019). Already, it has been estimated that dissociation of gas hydrates located on Arctic shelves contributes 0.08-0.13 Tg of methane per year to the atmosphere (McGuire et al., 2009).

Methane in marine sediment is significantly depleted in ^{13}C, often having a stable carbon isotope composition ($\delta^{13}C$) less than <-40 ‰ (Whiticar, 1999). In areas characterized by upward methane seepage, consumption of this methane by aerobic and anaerobic processes and the stable carbon isotope composition ($\delta^{13}C$) of DIC in bootom water and especially pore water and can become greately depleted in ^{12}C. Benthic foraminifera living on or just below the seafloor precipitate carbonate shells (or tests) using ambient dissolved inorganic carbon (DIC) (McCorkle et al., 1990). Benthic foraminifera have been widely used to reconstruct methane seepage at cold seeps andb gas hydrate-rich sediments (e.g., Wefer et al., 1994; Kennett et al., 2000; Hill et al., 2003; Barbieri and Panieri, 2004; Martin et al., 2007 and 2010, Panieri et al., 2009, 2012, 2014 and 2016; Consolaro et al., 2015; Schneider et al., 2018). However, it has been demonstrated that both benthic and planktonic foraminifera can be affected by diagenetic processes, particularly the secondary overgrowth precipitation of

68 methane derived authigenic carbonate (MDAC). While it is now accepted that MDAC
69 overgrowth alters the $\delta^{13}C$ of the formainiferal isotope record (Torres et al., 2003; Panieri et
70 al., 2016, 2017a; Schneider et al., 2017 and 2018; Consolaro et al., 2018; Wan et al., 2018),
71 the impact of such diagenesis on foraminiferal $\delta^{18}O$ is less clear. In studies involving hydrate
72 stability reconstructions, both the stratigraphy and climate variations are usually interpreted
73 basd on the foraminiferal d18O record (e.g., Dickens et al., 1995; Kenett et al., 2000; Thomas
74 et al., 2002). Nevertheless, the climate reconstruction approach is problematic in cold seeps
75 releasing methane from gas hydrate source, as one would expect considering that the water
76 trapped in gas hydrates is more enriched in ^{18}O compared to the adjacent pore water
77 (Davidson, 1983). During gas hydrate dissociation, ^{18}O-enriched water is released, and this
78 signal can potentially be incorporated in the shell precipitated by living benthic foraminifera.
79 In addition, this signal can be captured by the MDAC precipitating on the foraminiferal shell
80 after the death of the organisms (secondary overgrowth).
81 In this study, we investigate living and fossil foraminiferal specimens from different
82 cold seeps in the Arctic Ocean and the Norwegian Sea to understand if and how methane
83 release and/or hydrate dissociation can affect the foraminiferal $\delta^{18}O$ signature. We generate
84 new foraminiferal $\delta^{18}O$ data sets using living (Rose Bengal stained) and fossil benthic and
85 planktonic foraminiferal species (fractions >63 and >125 µm) from an active pockmark
86 currently releasing methane at Vestnesa Ridge, from gas hydrate mounds from Storfjordrenna
87 (south Svalbard) and from two canyons offshore the Lofoten islands (Northern Norway)
88 characterized by methane-rich sediments. We interpret the results obtained in the context of
89 the sampling environment (i.e, presence/absence of gas hydrates and methane seepage), but
90 also of the foraminiferal ontogeny and ecological preferences (i.e., microhabitat). Finally, we
91 compare the results obtained examining the $\delta^{18}O$ data together with $\delta^{13}C$ data from the same
92 samples. This study represents a significant advancement in the application of the
93 foraminiferal $\delta^{18}O$ in paleoclimatic reconstructions conducted at sites of methane release and
94 gas hydrate dissociation.
95
96 **2. Study area**
97 This study is based on sediment samples from push cores collected at three geographic
98 locations: 1) Vestnesa Ridge, western Svalbard margin (79°N, 6°E, 1200 m water depth), 2)
99 Storfjordrenna, south Svalbard margin (76°N, 16°E, ~390 m water depth); and 3) an area of
100 the Norwegian margin east of the Lofoten Islands (68°N, 10°W, ~750 m water depth) (Figs. 1

A-D; Table 1). Vestnesa Ridge is a 100 km-long sediment drift oriented SE-NW to E-W (Talwani and Eldholm, 1977; Thiede et al., 1998; Bünz et al., 2012) characterized by gas hydrate in the subseafloor and methane emitting pockmarks (Bünz et al., 2012; Panieri et al., 2017b). Storfjordrenna is a channel characterized by several mounds (~500 m in diameter and ~10 m in height above the seafloor) constituted by hemipelagic sediments with gas hydrate and carbonate layers of, referred to as gas hydrate mounds (GHM) (Hong et al., 2017, 2018) or gas hydrate pingos (Serov et al., 2017). The third geographic location comprises two canyons situated north of the Trænadjupet slide, on the southern part of the continental Lofoten-Vesterålen slope (Rise et al., 2013). These canyons are ~1.3 km long and 50 m deep relative to surrounding seafloor. Within the canyons, the seafloor is characterized by active methane seepage and microbial mats (Sen et al., 2019); however, there is no evidence for gas hydrates in this area (Rise et al., 2013; Hong et al., 2019).

3. Materials and Methods

3.1 Sediment core collection

Push cores from Vestnesa Ridge were collected in July 2016 using the R/V *G.O. Sars* and the ROV *Ægir 6000*. The sampling was conducted within the two most active pockmarks (Lunde and Lomvi; Figs. 1 A and B). In particular, we collected 7 push cores within the Lunde pockmark (cores V-15, V-16, V-17, V-18, V-19, V-21 and V-25) and 3 push cores within the Lomvi pockmark (cores V-7, V-8 and V-9) (Table 1). The sampling targeted whitish microbial mats (Figs. 1 F and G), indicative of active methane seepage. One push core was collected in the Lunde pockmark in sediments devoid of microbial mats and with no rising methane bubbles (core V-20; Fig. 1E). At this site, head space analysis confirmed the absence of methane. Because of this, we consider this a non-seep reference core.

Multicores from two gas hydrate bearing mounds (GHM) in Storfjordrenna (GHMs 1 and 5) were collected in June 2017 using the R/V Helmer Hanssen and a multicorer equipped with a video camera system (cores 898, 900, 902, 916, 917, 918, 919, 920, 921, and 922; Figs. 1 A and C; Table 1). The push cores from the Lofoten-Vesterålen (LV) canyons were collected in August 2017 during a cruise on board the R/V *G.O. Sars* using the ROV *Ægir 6000* (cores L-8, L-19, L-31, L-32, L-35, L-52, L-56; Figs. 1 A and D; Table 1).

3.2 Pore water analysis

Pore water samples were collected in all cores considered in this study, with the exception of cores V-15 and V-19 (Vestnesa Ridge), where we could not extract enough pore

water for sulfate analyses. All pore water samples were measured for sulfate (SO_4^{2-}) except cores 916, 920, 921, and 922 (Storfjordrenna) because of the low yield. In the LV area, the cores collected in the southern canyon were shared for macro-biology, geochemistry, and micropaleontology investigations. Thus, sulfate profiles were obtained from push cores adjacent to the cores studied for foraminifera. Sulfate concentrations were determined by a Dionex ICS-1100 Ion Chromatograph equipped with a Dionex IonPac AS23 column at the Norwegian Geological Survey (NGU, Trondheim, Norway; Sauer et al., 2016).

Chloride concentrations were measured on pore water samples from cores V-7, V-8, V-9, V-16, V-20, 898, 900, 902, 917, 918, and 919. Chloride concentrations were also determined from the LV canyons cores and reported in Hong et al., (2019). All chloride concentrations were measured onshore also by ion chromatograph (see analytical details in Yao et al. (2019).

The $\delta^{13}C_{DIC}$ was determined on every core analyzed for sulfate, with the exception of cores L-52 and L-56. Measurements were conducted at EAWAG (The Swiss Federal Institute of Aquatic Science and Technology) using an IRMS (Isotope Ratio Mass Spectrometer, Isoprime) equipped with a Gilson 222XL Liquid Handler and a Multiflow unit (Isoprime). Data are reported relative to the Vienna Pee Dee Belemnite (VPDB). The laboratory standard deviation for the VPDB $\delta^{13}C$ was ±0.1‰, based on repeated measurements of the standard. $\delta^{13}C_{DIC}$ from the LV area were measured at Oregan State University (see details for methods in Torres et al., 2005). All pore water raw data are available in supplementary Table a.

3.3 Foraminiferal stable isotope geochemistry

All cores for micropaleontological analysis were sliced on board. Specifically, we collected the first 5 cm of each core at 1-cm resolution at Vestnesa for foraminiferal analyses, with the exception of cores V-15 and V-20 for which only the first 2 cm and first cm, respectively, were available. The same has been done for the first sediment horizon (0-1 cm) in Storfjordrenna and LV samples. All samples were stored in a 2 g L^{-1} Rose Bengal solution in 96 % ethanol, in order to identify living individuals (Walton, 1952). Stained individuals were considered alive or recently alive following Corliss (1991). Prior to washing, samples were stored at 4° C for at least 14 days, following the FOBIMO protocol (Schönfeld et al., 2012), then wet sieved using 63 and 125 µm mesh sieves and dried at 40° C. Foraminifera were picked from the fractions >63 and >125 µm using a stereo microscope.

Isotope measurements ($\delta^{13}C$ and $\delta^{18}O$) were performed on Rose Bengal stained, dead benthic and dead planktonic foraminifera from the 0-1 cm interval of all cores collected at the three sampled geographic locations (Figs. 1 A-D). In addition, foraminiferal isotope data were collected from the 3-4 cm interval of the Vestnesa Ridge cores. This allowed the comparison of the foraminiferal isotope composition with the most superficial pore water $\delta^{13}C_{DIC}$ data available. On cores V-8 and V-16, the isotopic composition of foraminifera was measured for the entire length of the cores (i.e, 30 and 20 cm for cores V-8 and V-16, respectively).

Foraminiferal $\delta^{13}C$ and $\delta^{18}O$ measurements were conducted at the stable isotope laboratory at UiT – The Arctic University of Norway in Tromsø (Norway) using a Thermo Scientific MAT253 IRMS coupled to a Gasbench II. Species-specific analyses were done on several benthic (*Cassidulina neoteretis*, *Cibicides wuellerstorfi*, *Melonis barleeanus*, *Nonionellina labradorica* and *Trifarina earlandi*) and planktonic (*Neogloboquadrina pachyderma)* foraminiferal species. Recently, it was reported that *M. barleeanus* is characterized by sedimentary particles within its shell, but this mostly influence isotopic data collected using in-situ, rather than bulk, techniques (Borrelli et al., 2018). Foraminiferal shells were placed in 4.5 mL vials and flushed with He gas. Five drops of water-free H_3PO_4 were added manually. After equilibration (>3 hours at 50°C), the samples were analyzed on a Gasbench II and MAT253 Isotope Ratio Mass Spectrometer. Normalization to the VPDB for carbon and oxygen isotopes was done using in-house standards (1.96 ‰, -10.21 ‰, and -48.95 ‰ for $\delta^{13}C$ and -2.15 ‰ and -18.59 ‰ for $\delta^{18}O$). Analytical precision was estimated to be better than 0.07 ‰ for $\delta^{13}C$ and 0.08 ‰ for $\delta^{18}O$ by measuring the certified standard NBS-19. Foraminiferal $\delta^{13}C$ and $\delta^{18}O$ data are reported in supplementary Tables b, c, and d.

Selected specimens were examined by scanning electron microscopy (SEM) and energy dispersive x-ray spectrometry (EDS) to investigate possible diagenetic alterations of the shells. Analyses were performed on several benthic (*Cassidulina neoteretis*, *Melonis barleeanus*, *Nonionellina labradorica and Trifarina earlandi*) and on one planktonic (*Neogloboquadrina pachyderma*) foraminiferal species. 24 specimens have been analyzed and we selected 12 of them to show in this study, based on the quality of the images obtained. The analyzed specimens were chosen from different sediment depths (0-1 cm, 3-4 cm, and 29-30 cm) from cores collected at the three study areas. Specimens were mounted on a circular 25 mm diameter mold using adhesive tape. The mount was then carbon coated and examined with a SEM Hitachi Tabletop Microscope TM-3030 equipped with a Bruker Quantax 70 EDS Detector at UiT. Uncalibrated EDS analyses were performed on the same specimens imaged

by SEM to evaluate the elemental composition of the foraminiferal shells and secondary overgrowth.

4. Results

4.1 Pore Water profiles

At Vestnesa Ridge, sulfate concentrations remain fairly constant for core V-20 (our inactive, non-seep control core), and near those of seawater (~28 mM), ranging from 28.4 to 29.6 mM (Fig. 2). Sulfate concentrations in all other cores examined decrease sharply from the seafloor to the bottom of the core. We note that sulfate concentrations in cores V-9 and V-16 are much lower than seawater values, even close to the seafloor (3.6 mM at 2 cm depth and 8.1 mM at 1 cm depth for cores V-9 and V-16, respectively). Except for cores V-18 and V-21, sulfate concentrations are undetectable by 10 cm sediment depth (Fig. 2).

In cores from Storfjordrenna GHM1 (Fig. 3), sulfate profiles at the tops of core have sulfate concentrations similar to that of seawater, with the exception of core 902, where it is 20.2 mM. Sulfate concentrations remain almost constant with depth in cores 898, 917, and 919. A sharp decrease in sulfate concentration with depth is observed in core 902, where sulfate reaches 0.4 mM at 24 cm depth. In cores 900 and 918, sulfate concentration decreases with sediment depth, reaching 2.7 mM at 34 cm and 13.7 mM at 47 cm depth in core 900 and 918, respectively (Fig. 3).

In the LV area, sulfate concentrations were measured on cores from the northern canyon (L-52 and L-56) and from the southern canyon (L-8, L-19, L-31, L-32 and L-35) (Fig. 4). In the southern canyon, cores available for pore water analysis were adjacent to cores studied for foraminifera. Specifically, push core L-9 and push core L-12 were collected next to push cores L-8 and L-19, respectively, whereas push core L-30 was collected next to cores L-31, L-32, and L-35 (Table 1). Overall, the LV canyons cores are characterized by a sharp decrease of sulfate with increasing sediment depth, with the exception of core L-12, which shows constant sulfate concentrations similar to seawater values. In the northern canyon, sulfate reaches very low concentrations around 12 cm depth (cores L-52 and L-56). In the southern canyon, sulfate concentrations are lower than 1 mM below 2 cm in core L-9 and below 6 cm in core L-30 (Fig. 4).

Chloride concentration ranges between 500 and 600 mM and it remains almost constant regardless of sediment depth in all cores analyzed (Figs. 2 and 3). The $\delta^{13}C_{DIC}$ shows values close to 0 in cores V-20 and 898, reflecting the $\delta^{13}C_{DIC}$ signature of normal marine

233 environment (-1 to 1‰; Tagliabue and Bopp, 2008). The $\delta^{13}C_{DIC}$ ranges between -20 and -50
234 ‰ in the cores collected at Vestnesa Ridge and Storjordrenna GHM1, whereas the cores
235 collected at the LV canyons are characterized by $\delta^{13}C_{DIC}$ values between -10 ‰ and -70 ‰
236 (Figs. 2-4).
237
238 **4.2 Foraminiferal isotopic composition**
239 In this study, we primarly focus on samples collected at Vestnesa Ridge. The presence
240 of gas hydrates at the seafloor and associated gas seepages in the area (Vogt et al., 1994;
241 Hutsoft et al., 2009; Petersen et al., 2010; Bünz et al., 2012; Panieri et al., 2017b), together
242 with the the fact that the cores were collected on microbial mats using a remotely operated
243 vehicle (ROV), make these samples the ideal ones to study the potential effect of gas hydrate
244 dissociation on the foraminiferal $\delta^{18}O$ signature. Hence, at Vestnesa Ridge, we generated
245 complete foraminiferal stable isotope data sets using samples from cores V-8 (30 cm long)
246 and V-16 (20 cm long) (Figs. 1B and 5). We selected these two cores because of the high
247 number of living and dead individuals belonging to *N. pachyderma*, *M. barleeanus*, and *C.*
248 *neoteretis*. The foraminiferal isotopic composition of *N. pachyderma*, *C. neoteretis* and *M.*
249 *barleeanus* was also measured in core V-20, in the interval 0-1 cm (Vestnesa Ridge; Figs. 1B
250 and 5). These values represent the isotopic composition of foraminifera not affected by
251 methane release and oxidation.
252 The foraminiferal $\delta^{13}C$ values from core V-20 are similar to the foraminiferal $\delta^{13}C$
253 typical of normal marine conditions (-1 to 1‰; McCorkle et al., 1990), whereas the $\delta^{18}O$
254 values range from 2.7 to 2.8 ‰ (*N. pachyderma*) and from 4.3 to 4.5 ‰ (*C. neoteretis),* with
255 *M. barleeanus* recording values from 3.9 to 4 ‰, which are very close to benthic and
256 planktonic values measured in the area (e.g., Consolaro et al., 2017, Schneider et al., 2018).
257 In samples from cores V-8 and V-16, the *M. barleeanus* $\delta^{13}C$ values range from -2 to -
258 8 ‰, whereas *N. pachyderma* is characterized by values between 1.2 and -14 ‰. In core V-8,
259 we analyzed also *C. neoteretis* and its $\delta^{13}C$ values range from -1.5 to -16 ‰. In general, the
260 foraminiferal $\delta^{13}C$ decreases with increasing sediment depth at core V-8, whereas at core V-
261 16, the $\delta^{13}C$ values decreases from the core surface to a depth of 10 cm and increases
262 afterwards. The trend in foraminiferal $\delta^{18}O$ values is less straightforward. In core V-8, *N.*
263 *pachyderma* $\delta^{18}O$ ranges from 0.2 to 4.4 ‰, with higher values below 11 cm. On the other
264 hand, the *M. barleeanus* $\delta^{18}O$ ranges from 3.9 to 4.3 ‰, with no trend with increasing
265 sediment depth. The *C. neoteretis* $\delta^{18}O$ varies from 4.6 ‰ to 5.0 ‰ and shows a slight

increase with increasing sediment depth. In core V-16, relatively higher $\delta^{18}O$ values were measured in *N. pachyderma* and *M. barleeanus* in samples close to the sulfate methane transiton (SMT). Below this depth, the $\delta^{18}O$ values decrease only slightly. The *N. pachyderma* $\delta^{18}O$ ranges from 2.3 to 4.2 ‰, whereas the range of *M. barleeanus* $\delta^{18}O$ values is 4.0 to 4.6 ‰.

For cores V-8, V-16, and V-20, isotopic measurements were conducted on planktonic and benthic species from the size fractions >63 µm and >125 µm. Our results do not show a size fraction effect on the $\delta^{18}O$ and $\delta^{13}C$ data. Specifically, a difference of less than 3 % and 6 % difference for $\delta^{18}O$ and $\delta^{13}C$, respectively, is measured between the two size fractions analyzed. The only exception is represented by *M. barleeanus* samples, for which a slight difference between the fractions >63 and >125 µm is observed for the core V-16 $\delta^{13}C$ record.

Additional analyses were conducted on samples from all the other cores collected at Vestnesa Ridge, Storjordrenna, and the LV canyons (Figs. 1 and 6; Table 4). In superficial samples (0-1 cm; Fig. 6A), planktonic foraminiferal $\delta^{18}O$ values are heavier in the GHM Storfjordrenna samples (3-4 ‰) compared to the Vestnesa and LV ones (< 3 ‰). On the contrary, *M. barleeanus* $\delta^{18}O$ values are heavier in cores from Vestnesa Ridge (> 4 ‰ in most of the cores) than in cores from the other sampled areas. The range of $\delta^{18}O$ values is significantly variable in these samples, with planktonic $\delta^{18}O$ values of 1.0 – 4.5 ‰ and benthic $\delta^{18}O$ values of 3.7 – 5.6 ‰. The isotopic signal recorded on living individuals (*C. wuellerstorfi*, *C. neoteretis* and *M. barleeanus*) from Vestnesa Ridge and GHM Storfjordrenna cores does not clearly differ from the values measured in dead foraminifera from the same samples (living-dead difference of 0.6 ‰ for $\delta^{13}C$ and 0.5 ‰ for $\delta^{18}O$).

We note that lower $\delta^{18}O$ values are measured in cores from the LV sites, where heavier benthic (*T. earlandi)* and planktonic (*N. pachyderma*) $\delta^{18}O$ values (2.5 – 3 ‰) coincide to more negative $\delta^{13}C$ values (down to -34.1 ‰). This relationship seems to be present also in the deeper (3-4 cm) samples from Vestnesa Ridge (Fig. 6B), where heavier benthic and planktonic foraminiferal $\delta^{18}O$ (4.5 – 5.5 ‰) coincide to $\delta^{13}C$ values of -11.6 ‰ (*C. neoteretis*) and -15.2 ‰ (*N. pachyderma*). In cores V-8, V-16, and V-20, a similar correspondence between higher $\delta^{18}O$ values and lower $\delta^{13}C$ values is present as well (Fig. 5).

4.3 Foraminiferal microscopy and spectroscopy analyses

Scanning electron microscopy and EDS investigations revealed pristine shells (shells not affected by diagenesis) in superficial samples (0-1 cm) from Vestnesa Ridge and

Storfjordrenna (i.e, *C. neoteretis, M. barleeanus, N. labradorica,* and *N. pachyderma;* Figs. 7 A, E, G, and I). Altered shells (shells characterized by carbonate secondary overgrowth) are identified from the 3-4 cm interval of samples collected at Vestnesa Ridge (*C. neoteretis*, *M. barleeanus*, *N. labradorica*, and *N. pachyderma*; Figs. 7 B, C, D, F, H, and J). Unexpectedly, we found the presence of diagenetic alterations on foraminifera shells in superficial samples (0-1 cm) from cores collected at the LV canyons (*N. pachyderma* and *T. earlandi;* Figs. 7 K and L).

The EDS semi-quantitative analysis show low Mg concentrations in pristine shells (Figs. 7 A, E, and G), even if the EDS map of *N. pachyderma* from core V-8 (0-1 cm; Fig. 7I) reveals a region of high Mg content. Compared to pristine shells, shells affected by diagenesis are characterized by higher Mg concentrations (Figs. 7B, C, D, F, H, and J), with the exception of the superficial samples from the LV canyons where spots of high Ba, rather than Mg, were observed (Figs. 7K and L).

5. Discussion and conclusions

5.1 Geochemical characteristics of gas hydrate and methane-rich sediments

Regions of the seafloor with significant methane are characterized by opposing gradients of pore water sulfate and methane that intersect at a SMT. This is because upward migrating methane can react with sulfate through microbially-mediated anaerobic oxidation of methane (AOM; e.g., Boetius et al., 2000). At the broad scale, the depth of the SMT, though affected by numerous factors, mostly relates to the flux of upward methane (Bhatnagar et al., 2008).

The sharp decrease in sulfate concentration with sediment depth suggests that the SMT is within the first 10 cm in most cores from Vestnesa Ridge except for the inactive, non-seep control core (Fig. 2). The SMT is close to the seafloor in Vestnesa cores V-7, V-8, V-9 and V-16 (less than 10 cm) indicating high methane fluxes putatively advective (Yao et al., 2019). On the contrary, the reference core V-20 displays a sulfate profile typical for marine environments, with no methane influence (Borowski et al., 1996). At Storfjordrenna GHM1, sulfate profiles indicate a deeper SMT (tens of cm), with several cores unable to penetrate the SMT (Fig. 3). In the LV canyons (Fig. 4), the SMT seems close to the seafloor (~5 cm) in the southern canyon, with the exception of core L-12, deeper (10-15 cm) in the northern canyon (core L-52).

The AOM reaction produces hydrogen sulfide and bicarbonate, the latter which comprises most of DIC in marine settings. Universally, the DIC in sediment pore waters is

depleted in ^{13}C around SMT (e.g., Torres et al., 2003; Ussler et al., 2008), due to both the ^{13}C-depleted methane as the carbon source and isotopic fractionation associated with this microbial process (Borowski et al., 1997; Hong et al., 2013; Yoshinaga et al., 2014). The actual $\delta^{13}C$ value of DIC at the SMT is complicated. Methane can derive from thermogenic ($\delta^{13}C$: -55 ‰ to -40 ‰) or microbial ($\delta^{13}C$: -100 ‰ to -55 ‰) sources (Whiticar, 1999); DIC enriched in ^{13}C and formed during methanogenesis can also migrate upward (Chatterjee et al., 2011).

The $\delta^{13}C_{DIC}$ profiles (Figs. 2-4) reveal depleted values at cores V-7, V-8, V-9, V-16, V-17, V-18, and V-21 from Vestensa Ridge; cores 900, 902, 917, 918, and 919 from Storfjordrenna, and cores L-9, L-12, and L-30 from the LV canyons. Core V-20 is the only core at Vestnesa Ridge that records the $\delta^{13}C_{DIC}$ values similar to modern normal marine environment (-1 to 1‰; Tagliabue and Bopp, 2008), confirming that this core is not affected by methane seepage and oxidation. Core 898 also shows $\delta^{13}C_{DIC}$ values similar to the modern normal marine environment. In all other cores investigated, the negative $\delta^{13}C_{DIC}$ values suggest that cored sites are influenced by upward methane fluxes (e.g., Whiticar et al., 1999). In GHM cores, we cannot exclude a signal reflecting organiclastic sulfate reduction, which occurs between the seafloor and the SMT and is characterized by depleted but greater $\delta^{13}C_{DIC}$ than AOM (Chatterjee et al., 2011).

The chloride profiles available from Vestnesa Ridge and Sorfhordrenna GHM1 (Figs. 2 and 3) do not vary with sediment depth, suggesting that the sampling sites are not affected by fluid migration of a low-chloride fluid through the sediment column.

5.2 Foraminiferal evidences of gas hydrate emission

5.2.1 Foraminiferal stable isotope compositions

Overall, the isotopic compositions of Rose Bengal stained ('living') foraminifera do not substantially differ from other values reported in literature. In fact, specimens of *C. neotretis* and *N. pachyderma* from the top of the control core V-20 (0-1 cm; Fig. 5), which has no evidence for upward methane migration, exhibit values consistent with other studies in the region (e.g., Consolaro et al., 2015; Schneider et al., 2018). There is also a clear distinction between planktonic and benthic $\delta^{13}C$ and $\delta^{18}O$ values. Vital effects and ecological preferences (e.g., microhabitat), but also environmental parameters (e.g., temperature, pH), all influence the isotopic composition of the foraminiferal shells (Duplessy et al., 1970; Bemis et al., 1998; Ravelo and Hillaire Marcel, 1999; Barras et al., 2010). In this context, we interpret the offset

between the $\delta^{18}O$ of *C. neotretis* and *N. pachyderma* as a consequence of different habitats for these species (e.g., Kennett et al., 2000; Consolaro et al., 2015). Ecological preferences (Murray, 2006) might also explain the small differences in stable isotope compositions between *C. neoteretis* (a shallow infaunal species) and *M. barleeanus* (an intermediate infaunal species). Notably, the former has higher $\delta^{13}C$ and $\delta^{18}O$.

However, of all foramifera samples examined, the most depleted $\delta^{13}C$ value (-5.7 ‰) was measured in Rose Bengal stained *N. labradorica*, a deep infaunal species (Racine et al., 2018). We note that the depleted $\delta^{13}C$ value we measured in this species is similar to the $\delta^{13}C$ signature measured in another living deep infaunal foraminifer from Monterey Bay (*Globobulimina pacifica;* -6 ‰; Bernhard et al., 2010). We believe that these $\delta^{13}C$ values represent a 'threshold' of the isotopic composition of non-diagenetically altered foraminifera inhabiting seep sites. It might be possible that the depleted $\delta^{13}C$ measured in our living *N. labradorica* is a consequence of vital effects. However, considering the sampling location, we think that the *N. labradorica* $\delta^{13}C$ is the result of the incorporation of methane derived ^{13}C-depleted carbon during shell formation and likely ingestion of ^{13}C-depleted methanotrophic microbes (Rathburn et al., 2003; Panieri, 2006; Bernhard and Panieri, 2018).

In gas hydrate bearing sediments, the $\delta^{18}O$ of pore water can be affected by gas hydrate formation and dissociation because the water trapped in gas hydrates is more enriched in ^{18}O compared to the adjacent pore water (Davidson et al., 1983; Tomaru et al., 2006; Ijiri et al., 2018). With the data available, we cannot draw a firm conclusion regarding the possibility that the $\delta^{18}O$ signature of living benthic foraminifera can record episodes of gas hydrate dissociation. Our data indicate that living foraminifera cannot record gas hydrate dissociation as shell formation is a discontinuous and brief process that might not be coeval with episodes of gas hydrate decomposition, which are also transient in time (Thatcher et al., 2013; Anderson et al., 2014). It might be equally possible that the $\delta^{18}O$ signature of living benthic foraminifera does not reflect the influence of gas hydrate dissociation, because no dissociation happened during the life span of the specimens analyzed. However, a different interpretation can be drawn when considering foraminifera with diagenetic overgrowth.

Over relatively long time scales (Plio-Peistocene), gas hydrate dissociation can alter the carbonate system and the MDAC isotopic signature (Bohrmann et al., 1998; Crémière et al., 2016), as revelaed by a recent study showing a disequilibrium between carbonate crust clumped isotopes and the expected temperature of formation (Loyd et al., 2016). In cores V-8 and V-16, the slight downcore increase in the *C. neoteretis* and *M. barleeanus* $\delta^{18}O$ (up to 5

‰) values compared to the reference-like values of core V-20 suggest the possible influence of gas hydrate dissociation on the $\delta^{18}O$ signature of fossil foraminifera through sedimentary overgrowth. The variability in the *N. pachyderma* $\delta^{18}O$ values (1.8 to 4.5 ‰) from cores V-8 and V-16 supports this hypothesis.

It was proposed that the planktonic foraminiferal isotopic composition can be influenced by hydrate dissociation (Maslin et al., 2005). However, in this work, the precipitation of authigenic carbonate around the foraminiferal shells was not discussed. Cores V-8 and V-16 are located at ~1,200 m water depth. Thus, methane seepage at these locations is rapidly dispersed in the ocean or microbially oxidized to CO_2 in the water column (Damn et al., 2005; Steinle et al., 2015), making it improbable that living planktonic foraminifera can record episodes of gas hydrate dissociation and methane oxidation (e.g., Consolaro et al., 2018). However, evidence of gas hydrate dissociation can be recorded after the death and burial of planktonic species, in particular at the depth of the SMT, where MDAC can precipitate on the foraminiferal shells (Panieri et al., 2016; Schneider et al., 2018).

In this study, the wide range of $\delta^{18}O$ values measured in both planktonic and benthic foraminiferal shells confirms that the isotopic composition of *N. pachyderma* and *C. neoteretis* is a consequence of the precipitation of ^{18}O-rich authigenic carbonates (see also next section). Our conclusion is in agreement with other studies conducted at different geographic locations (Fig. 6). For example, Torres et al. (2003) estimated that the range of $\delta^{18}O$ values (0-1.75 ‰) measured on foraminiferal calcite from the Hydrate Ridge was due to 22 wt.% (authigenic) carbonates precipitated around the shells. Heavier foraminiferal $\delta^{18}O$ (range from 2 to 4 ‰) were reported also for dead foraminifera from methane vents environments in the Gulf of California (Herguera et al., 2014). Also in this case, the foraminiferal isotopic composition was interpreted to be influenced by authigenic carbonates. Those results are in agreement with the range of data measured in our study areas (Fig. 6A). At Vestnesa Ridge, the identification of authigenic carbonate precipitated on foraminiferal tests from deeper sediments (several meters of sediment depth) points out the same depleted $\delta^{13}C$ and heavy $\delta^{18}O$ (Schneider et al., 2017; Fig. 6B).

Secondary overgrowth affected planktonic and benthic foraminifera alike, even if the ^{18}O enrichment is more evident in *N. pachyderma* because of the lower $\delta^{18}O$ values recorded by this species in marine environments not affected by methane (e.g. core V-20). In addition, similar $\delta^{18}O$ enrichments to the ones we measured in foraminifera were reported for MDAC

from gas hydrate and cold seeps settings (Greinert et al., 2001, 2010; Eichhubl and Boles, 1998; Eichhubl et al., 2000; Naehr et al., 2007, 2009; Crémière et al., 2016).

Gas hydrate dissociation, and consequent release of ^{18}O-enriched water is a process that takes place below the SMT, wile ^{13}C-depleted methane is present within the SMT. This would suggest that gas hydrate dissociation might not be associated with foraminiferal low $\delta^{13}C$ and high $\delta^{18}O$ values. However, our results clearly show a relationship between depleted $\delta^{13}C$ and enriched $\delta^{18}O$ values in foraminifera, in particular in cores V-8 and V-16, collected at gas hydrate bearing sediments where the SMT is close to the seafloor (Fig. 5).

We recognize that the foraminiferal $\delta^{18}O$ can vary because of changes in environmental parameters that are unrelated to gas hydrate dissociation. However, we do not think that this is the case for the samples analyzed in this study for several reasons. First, we observe a wide range of $\delta^{18}O$ values on both planktonic and benthic foraminifera even within the first few centimenters of sediment (Figs. 5 and 6). At Vestnesa Ridge, this difference in $\delta^{18}O$ values would translate in several degrees C difference in less than a millennium, if we take into account the modern sedimentation rate at this location (~19 cm/kyrs; Consolaro et al., 2015). We think that such a big temperature change in a short time frame is highly unlikely. In fact, this change would be more abrupt than temperature shifts characterizing the Heinrich events over the Pliocene (Cortijo et al., 1997). We note that a similar variability in the foraminiferal $\delta^{18}O$ as recorded in the Vestnesa Ridge samples was measured in surface sediments from the LV canyons (0-1 cm; Fig. 6A), confirming that a temperature change cannot be a likely explanation of our data, within the same 1 cm-sediment layer.

Second, similar foraminiferal $\delta^{18}O$ ranges from cold seep sites as the ones recorded in surface samples at Vestnesa Ridge (Fig. 6A) have not often been reported in literature, with a few exceptions possible as a consequence of temperature changes among the sites analyzed (e.g., 2 ‰ in Sen Gupta and Aharon, 1994; 1.35 ‰ in Burkett et al., 2018). Burkett et al. (2018) observed a maximum $\delta^{18}O$ increase of +0.7 ‰ in cold seeps that they interpreted to be the consequence of fluids impact. Considering our stable Chloride profiles together with the heat flow estimated in the Vestnesa Ridge, leading to heat excess of less than 0.04°C at 50 cm sediment depth (Bohrmann et al., 2016), we exclude this hypothesis.

Third, clay dehydration through the smectite transformation into illite can cause a ^{18}O enrichment of pore waters. This diagenetic process occurs in deep sediments at temperature ranging from 60° to 160° C (~1000 m below sea floor). However, the Chloride profiles at Vestnesa Ridge and Storfjordrenna GHM do not support any clay dehydration, as observed

464 also in mud volcano systems (Hensen et al., 2004). Yet, we cannot exclude an impact of
465 meteoric fluids in the LV canyons, as documented by Hong et al. (2019), with a different $\delta^{18}O$
466 signature, even though the correlation between depleted $\delta^{13}C$ and heavy $\delta^{18}O$ points to the
467 presence of authigenic carbonate on foraminiferal shells. Consequently, we do not think that
468 clay dehydration, temperature, or salinity changes can affect the pore water of surface
469 sediments in our three study areas.
470 Finally, the size fraction analyzed might also cause biases in the isotopic records used
471 to interpret short time-scale processes because the isotopic composition of large foraminifera
472 (>150 µm) can reflect a longer-term averaged calcification process that is not influenced by
473 episodic processes (i.e, eutrophic periods or seasonal changes; Fontanier et al., 2006). In
474 addition, ontogenic effects are reported in literature for both planktonic (e.g., Spero et al.,
475 1997; Elderfield et al., 2002) and benthic (e.g., Friedrich et al., 2006; Barras et al., 2010;
476 Schumacher et al., 2010) foraminifera. The analysis of different size fractions (150, 250, 350,
477 450, 550, 650 and 750 µm) by Corliss et al. (2002) did not reveal a seasonal influence on the
478 foraminiferal isotopic record, suggesting the absence of an ontogenetic effect on the
479 foraminiferal isotope incorporation. The foraminiferal isotope data we collected using
480 different size fractions (i.e., >63 and >125 µm) are in agreement with the conclusions reached
481 by Corliss et al. (2002), demonstrating that the benthic and planktonic foraminiferal $\delta^{18}O$
482 values are very similar in both fracions analyzed and that they are not biased by ontogenetic
483 effects.
484
485 **5.2.2 Foraminiferal secondary overgrowth**
486 Our SEM analyses revealed significant visual diagenetic alteration on several of the
487 foraminiferal shells analyzed, but not on all of them. Living individuals of *N. labradorica* and
488 *M. barleeanus* from Storfjordrenna GHM1 (Figs. 7 E and G) were not affected by diagenetic
489 alteration, even if we measured relatively low $\delta^{13}C$ in these samples. This suggest that the
490 depleted $\delta^{13}C$ signature of these samples was incorportated in the primary foraminiferal
491 calcite (calcite deposited by the foraminifera during shell growth), as proposed in other
492 studies (e.g., Panieri et al., 2017a, Schneider et al., 2017; Wan et al., 2018).
493 Diagenetic features were confirmed by EDS maps of samples collected deeper in the
494 sediment column. In particular, we interpret the high Mg concentration to be the evidence of
495 the presence of secondary overgrowth on the shells analyzed (e.g., Panieri et al., 2017a;
496 Schneider et al., 2017). In the 3-4 cm sediment horizon, diagenetic alterations were observed

497 in different Vestnesa pockmarks (*C. neoteretis* from cores V-8 and V-16; Fig. 7 B and C),
498 suggesting that precipitation of MDAC on foraminiferal shells occurs at a regional scale. The
499 *C. neoteretis* collected at deeper sediment depths (core V-8, 29-30 cm; Fig. 7D) is
500 characterized by the highest Mg content.
501 The samples from the LV canyon south did not reveal high concentrations of Mg, but
502 an enrichment in Ba (Fig. 7 K and L). Ba-calcite has been described as a product of early
503 diagenesis (Dejonghe and Boulvain, 1993; Schroeder et al., 1997), which can affect
504 foraminiferal carbonate (Lea and Boyle, 1993). Barite in seafloor crusts as well as high
505 dissolved Ba concentration have been described in the LV area (Sen et al., 2019; Hong et al.,
506 2019) and EDS analysis of foraminiferal shells show an initial possible precipitation of
507 authigenic Ba-rich overgrowth. Further investigations are needed to understand if these
508 overgrowths can impact the foraminiferal isotopic composition in samples from the LV
509 canyons and other geographic locations. Overall, our microscopy and spectroscopy analyses
510 confirm the hypothesis that the isotopic composition measured in fossil foraminifera is
511 affected by secondary overgrowth precipitated on the foraminiferal shells at the SMT and that
512 this signal is related to methane oxidation and gas hydrate dissociation.
513 Nevertheless, isotopic composition of fossil foraminifera might also depend on the
514 secondary overgrowth mineralogy. In fact, the mineralogy of MDAC usually include
515 microcrystalline Mg-calcite, aragonite, and dolomite (e.g., Roberts and Aharon, 1994,
516 Bohrmann et al., 1998, Crémière et al., 2012; Sauer et al., 2017). Different types of carbonate
517 have different oxygen isotopic fractionation (e.g., Kim et al., 2007; Vasconcelos et al., 2005).
518 For example, dolomite is estimated to show an enrichment of 5 to 7 ‰ of ^{18}O compared to
519 synthetic calcite (O'Neil and Epstein, 1966). At methane cold seeps, a wide range of $\delta^{18}O$ has
520 been related to the mineralogy of authigenic carbonates (e.g., Orphan et al., 2004; Gieskes et
521 al., 2005), with $\delta^{18}O$ values up to 7.5 ‰ in high Mg-calcite, while aragonite displayed lighter
522 $\delta^{18}O$.
523 The ^{18}O enrichment in authigenic carbonate rocks has been interpreted as evidence for
524 gas hydrate dissociation at several methane seep and non-seep environments (e.g., Bohrmann
525 et al., 1998: Aloisi et al., 2000; Pierre et al., 2002; Conti et al., 2004). At these sites, the heavy
526 $\delta^{18}O$ of Mg-calcite was used as an evidence for gas hydrate dissociation, whereas the origin of
527 light aragonite $\delta^{18}O$ remains uncertain. It is possible that this difference is a consequence of
528 Mg-calcite and aragonite precipitating from two highly distinct pore-water conditions
529 (Bohrmann et al., 1998), even if the chemical controls on the carbonate phase that precipitates

530 are still not completely understood (Burton, 1993). Schneider et al. (2017) estimated that the
531 authigenic carbonate proportion on foraminiferal tests can be up to 58 %. A calcite containing
532 50 % of Mg-$CaCO_3$ is expected to be enriched in ^{18}O by 3-4 ‰ (Tarutani et al., 1969; Fritz
533 and Smith, 1970).
534 Finally, in this study, we demonstrate that at methane seeps and gas hydrate bearing
535 sediments fossil planktonic and benthic foraminifera are characterized by relatively high $\delta^{18}O$
536 values. We propose that this ^{18}O enrichment is related to past gas hydrate dissociation
537 event(s). Hydrate dissociation release ^{18}O-enriched water, which affect the pore water isotopic
538 signature. This signal can be incorporated by authigenic carbonates precipitating around
539 foraminiferal shells at the SMT. In addition, we speculate that mineralogy of the secondary
540 overgrowth might also influence the isotopic signal measured in fossil foraminifera.
541
542 **Acknowledgments**
543 The authors wish to thank the captain and the crew of the R/V G.O. Sars and Helmer
544 Hanssen. This study has been funded by the project Petromaks2 Norcrust – Norwegian
545 margin fluid systems and methane-derived authigenic carbonate crusts (project no. 255150)
546 and the Research Council of Norway through CAGE Center for Excellence in Arctic Gas
547 Hydrate Environment grant 287 no. 223259.
548
549 **References**

550 Aloisi, G., Pierre, C., Rouchy, J.-M., Foucher, J.-P., Woodside, J., the MEDINAUT Scientific
551 Party, 2000. Methane-related authigenic carbonates of eastern Mediterranean Sea mud
552 volcanoes and their possible relation to gas hydrate destabilization. Earth and Planetary
553 Science Letters 184, 321-338. https://doi.org/10.1016/S0012-821X(00)00322-8.

554 Anderson, B., Boswell, R., Collett, T.S., Farrell, H., Ohtsuki, S., White, M., Zyrianova, M.,
555 2014. Review of the findings of the Ignik Sikumi CO_2-CH_4 gas hydrate exchange field trial.
556 In: Proceedings of the international conference on gas hydrates, Beijing; 2014.

557 Barras, C., Duplessy, J.-C., Geslin. E., Michel, E., Jorissen, F.J., 2010. Calibration of $\delta^{18}O$ of
558 cultured benthic foraminiferal calcite as a function of temperature. Biogeosciences 7, 1349-
559 1356.

Barbieri, R. and Panieri, G., 2004. How are benthic foraminiferal faunas influenced by cold seeps? Evidence from the Miocene of Italy. Palaeogeography, Palaeoclimatology, Palaeoecology 204, 257-275.

Bemis, B.E., Spero, H.J., Bijma, J., Lea D.W., 1998. Reevaluation of the oxygen isotopic composition of planktonic foraminifera: experimental results and revised paleotemperature equations. Paleoceanography 13 (2), 150 – 160.

Bernhard, J.M. and Panieri, G., 2018. Keystone Arctic paleoceanographic proxy association with putative methanotrophic bacteria. Scientific Reports 8, 10610.

Bernhard, J.M., Martin, J.B., Rathburn, A., 2010. Combined carbonate carbon isotopic and cellular ultrastructural studies of individual benthic foraminifera: 2. Toward an understanding of apparent disequilibrium in hydrocarbon seeps. Paleoceanography 25, PA4206, doi:10.1029/2010PA001930

Bhatnagar, G., Chapman, W.G., Dickens, G.R., Dugan, B., Hirasaki, G.J., 2008. Sulfate-methane transition as a proxy for average methane hydrate saturation in marine sediments. Geophysical Research Letters 35, L03611. doi:10.1029/2007GL032500.

Boetius, A., Ravenschlag, K., Schubert, C. J., Rickert, D., Widdel, F., Gieseke, A., Amann, R., Jorgensen, B. B., Witte, U., and Pfannkuche, O., 2000. A marine microbial consortium apparently mediating anaerobic oxidation of methane, Nature, 407, 623-626.

Bohrmann, G., Greinert, J., Suess, E., Torres, M., 1998. Authigenic carbonates from the Cascadia subduction zone and their relation to gas hydrate stability. Geology 26, 647-650. https://doi.org/10.1130/0091-7613(1998)026<0647:ACFTCS>2.3.CO;2.

Bohrmann, G., Ahrlich, F., Bergenthal, M., Bünz, S., Düßmann, R,. Ferreira, Ch., Freudenthal, T., Fröhlich, S., Hamann, K., Hong, W.-L., Hsu, Ch.-W., Johnson, J., Kaszemeik, K., Kausche,A., Klein, T., Lange, M., Lepland, A., Malnati, J., Meckel, S., Meyer-Schack, B., Noorlander, K., Panieri, G., Pape, T., Reuter, M., Riedel, M., Rosiak, U., Schmidt, Ch., Schmidt, W., Seiter, Ch., Spagnoli, G., Stachowski, A., Stange, N., Wallmann, K., Wintersteller, P., Wunsch, D., Yao, 2016. H.R/V MARIA S. Merian Cruise Report MSM57: http://nbn-resolving.de/urn:nbn:de:gbv:46-00105895-15

588 Borowski, W.S., Paull, C.K., Ussler, W., 1996. Marine pore-water sulfate profiles indicate in
589 situ methane flux from underlying gas hydrate. Geology 24, 655-658.

590 Borowski, W. S., Paull, C. K., and Ussler, W., 1997. Carbon cycling within the upper
591 methanogenic zone of continental rise sediments: An example from the methane-rich
592 sediments overlying the Blake Ridge gas hydrate deposits, Marine Chemistry, 57, 299-311.

593 Borrelli, C., Panieri, G., Dahl, T.M., Neufeld, K., 2018. Novel biomineralization strategy in
594 calcareous foraminifera. Scientific Reports 8, 10201.

595 Bünz, S., Polyanov, S., Vadakkepuliyambatta, S., Consolaro, C., Mienert, J., 2012. Active gas
596 venting through hydrate-bearing sediments on the Vestnesa Ridge, offshore W Svalbard.
597 Marine Geology 332–334, 189–197. http://dx.doi.org/10.1016/j.margeo.2012.09.012.

598 Burkett, A.M., Rathburn, A., Elena Pérez, M., Martin, J.B., 2018. Influences of thermal and
599 fluid characteristics of methane and hydrothermal seeps on the stable oxygen isotopes of
600 living benthic foraminifera. Marine and Petroleum Geology 93, 344-355.

601 Burton, E.A., 1993. Controls on marine carbonate cement mineralogy: Review and
602 reassessment. Chemical Geology 105, 163–179.

603 Chatterjee, S., Dickens, G. R., Bhatnagar, G. Chapman, W. G., Dugan, B., Snyder, G. T.,
604 Hirasaki, G.J., 2011. Pore water sulfate, alkalinity, and carbon isotope profilesin shallow
605 sediment above marine gas hydrate systems:A numerical modeling perspective. Journal of
606 Geophysical Research 116, B09103. doi:10.1029/2011JB008290.

607 Consolaro, C., Rasmussen, T.L., Panieri, G., Mienert, J., Bünz, S., Sztybor, K., 2015. Carbon
608 isotope ($\delta^{13}C$) excursions suggest times of major methane release during the last 14 kyr in
609 Fram Strait, the deepwater gateway to the Arctic. Climate of the Past 11, 669–685.
610 http://dx.doi.org/10.5194/cp-11-669-2015.

611 Consolaro, C., Rasmussen, T.L., Panieri, G., 2018. Palaeoceanographic and environmental
612 changes in the eastern Fram Strait during the last 14,000 years based on benthic and
613 planktonic foraminifera. Marine Micropaleontology 139, 84-101.
614 https://doi.org/10.1016/j.marmicro.2017.11.001

615 Conti, S., Fontana, D., Gubertini, A., Sighinolfi, G., Tateo, F., Fioroni, C., Fregni, P., 2004. A
616 multidisciplinary study of middle Miocene seep-carbonates from the northern Apennine
617 foredeep (Italy). Sedimentary Geology 169, 1-19.

618 Corell, R.W., Hassol, S.J., Melillo, J., 2008: Emerging Challenges – Methane from the Arctic:
619 Global warming wildcard, UNEP Year Book 2008: An Overview of Our Changing
620 Environment, United Nations Environment Programme, Stevenage, Hertfordshire, UK.

621 Corliss, B.H. (1991), Morphology and microhabitat preference of benthic foraminifera from
622 the northwest Atlantic Ocean, Mar. Micropaleontology, 17(3-4), 195-236, doi:10.1016/0377-
623 8398(91)90014-W.

624 Corliss, B.H., McCorkle, B.C., Higdon, D.M., 2002. A time series study of the carbon
625 isotopic composition of deep-sea benthic foraminifera. Paleoceanography 17, 1-27.
626 https://doi.org/10.1029/2001PA000664.

627 Cortijo, E., Labeyrie, L., Vidal, L., Vautravers, M., Chapman, M., Duplessy, J.-C., Elliot, M.,
628 Arnold, M., Turon, J.-L., Auffret, G., 1997. Changes in sea surface hydrology associated with
629 Heinrich event 4 in the North Atlantic Ocean between 40° and 60°N. Earth and Planetary
630 Science Letters 146, 29-45.

631 Crémière, A., Pierre, C., Blanc-Valleron, M.-M., Zitter, T., Namik Çağatay, M., Henry, P.,
632 2012. Methane-derived authigenic carbonates along the North Anatolian fault system in the
633 Sea of Marmara (Turkey). Deep Sea Research Part I: Oceanographic Research Papers 66,
634 114-130.

635 Cremiere, A., Lepland, A., Chang, S., Sahy, D., Condon, D. J., Noble, S. R., Martma, T.,
636 Thorsnes, T., Sauer, S., and Brunstad, H., 2016. Timescales of methane seepage on the
637 Norwegian margin following collapse of the Scandinavian ice sheet, Nature communications.

638 Damm, E., Mackensen, A., Budeus, G., Faber, E., Hanfland, C., 2005. Pathways of methane
639 in seawater: Plume spreading in an Arctic shelf environment (SW-Spitsbergen). Continental
640 Shelf Research 25, 1453-1472.

641 Davidson, D. W., Leaist, D.G., Hesse, R., 1983. Oxygen-18 enrichment in the water of a
642 clathrate hydrate. Geochimica et Cosmochimica Acta 47, 2293-2295.

643 Dickens, G.R., J.R. O'Neil, D.K. Rea, and R.M. Owen (1995), Dissociation of oceanic
644 methane hydrate as a cause of the carbon isotope excursion at the end of the Paleogene,
645 Paleoceanography, 10(6), 965-971, doi:10.1029/95PA02087.

646 Duplessy, J.-C., Lalou, C., Claude Vinnot, A., 1970. Differential Isotopic Fractionation in
647 Benthic Foraminifera and Paleotemperatures Reassessed. Science 10, 250-251.

648 Eichhubl, P., Boles, J.R., 1998. Vein formation in relation to burial diagenesis in the Miocene
649 Monterey Formation, Arroyo Burro Beach, Santa Barbara, California. In: Eichhubl. P. (Ed.),
650 Diagenesis, Deformation, and Fluid Flow in the Miocene Monterey Formation of coastal
651 California. SEPM Pacific Section Special Publication 83, pp. 15–36.

652 Eichhubl, P., Greene, H. G., Naehr, T., Maher, M., 2000. Structural control of fluid flow:
653 offshore fluid seepage in the Santa Barbara Basin, California. Journal of Geophysical
654 Exploration 69-70, 545-549. https://doi.org/10.1016/S0375-6742(00)00107-2.
655
656 Elderfield, H., Vautravers, M., Cooper, M., 2002. The relationship between shell size and
657 Mg/Ca, Sr/Ca, δ18O, and δ13C of species of planktonic foraminifera. Geochenistry,
658 Geophiscs, Geosystems 3, 1-13.

659 Dejonghe, L., Boulvain, F., 1993. Paleogeographic and diagenetic context of a baritic
660 mineralization enclosed within Frasnian peri-reefal formations: Case history of the
661 Chaudfontaine mineralization (Belgium). Ore Geology Reviws 7, 413-431.

662 Duplessy, J.-C., Lalou, C., Vinot, A.C., 1970. Differential isotopic fractionation in benthic
663 foraminifera and paleotemperatures reassessed. Science 168, 250 – 251.

664 Fontanier, C., Mackensen, A., Jorissen, F.J., Anschutz, P., Licari, L., Griveaud, C., 2006.
665 Stable oxygen and carbon isotopes of live benthic foraminifera from the Bay of Biscay:
666 Microhabitat impact and seasonal variability. Marine Micropaleontology 158, 159-183.
667 https://doi.org/10.1016/j.marmicro.2005.09.004.

668 Friedrich, O., Schmiedl, G., Erlenkeuser, H., 2006. Stable isotope composition of Late
669 Cretaceous benthic foraminifera from the southern South Atlantic: Biological and
670 environmental effects. Marine Micropaleontology 58, 135-157.

671 Fritz and Smith, 1970. The isotopic composition of secondary dolomites, Geochimlca et
672 Cosmochimica Acta. 34, pp. 1101-1173.

673 Greinert, J., Bohrmann, G., Suess, E., 2001. Gas Hydrate-Associated Carbonates and
674 Methane-Venting at Hydrate Ridge: Classification, Distribution, and Origin of Authigenic
675 Lithologies. In: Paull CK, Dillon WP (eds) Natural gas hydrates: occurrence, distribution, and
676 detection. Geophysical Monograph series 124, 99–113.

677 Greinert, J., Bialas, J., Lewis, K., Suess, E., 2010. Methane seeps at the Hikurangi Margin,
678 New Zealand. Marine Geology 272, 1-3.

679 Gieskes, J., Mahn, C., Day, S., Martin, J. B., Greinert, J., Rathburn, T., McAdoo, B., 2005. A
680 study of the chemistry of pore fluids and authigenic carbonates in methane seep
681 environments: Kodiak Trench, Hydrate Ridge, Monterey Bay, and Eel River Basin. Chemical
682 Geology 220, 329-345. https://doi.org/10.1016/j.chemgeo.2005.04.002.

683 Hensen, C., Wallmann, K., Schmidt, M., Ranero, C.R., Suess, E., 2014. Fluid expulsion
684 related to mud extrusion off Costa Rica—A window to the subducting slab. Geology 32, 201-
685 204.

686 Herguera, J.C., Paull, C.K., Perez, E., Ussler, W., Peltzer, E., 2014. Limits to the sensitivity of
687 living benthic foraminifera to pore water carbon isotope anomalies in methane vent
688 environments. Paleoceanography 29, 273-289.

689 Hill, T.M., Kennett, J.P., Spero, H.J., 2003. Foraminifera as indicators of methane-rich
690 environments: A study of modern methane seeps in Santa Barbara Channel, California.
691 Marine Micropaleontology 49, 23-138.

692 Hong, W.-L., Torres, M. E., Kim, J.-H., Choi, J., and Bahk, J.-J., 2013. Carbon cycling within
693 the sulfate-methane-transition-zone in marine sediments from the Ulleung Basin,
694 Biogeochemistry, 1-20, 10.1007/s10533-012-9824-y.

695 Hong, W.-L., Torres, M.E., Carroll, J., Cremiere, A., Panieri, G., Yao, H., Serov, P., 2017.
696 Seepage from an Arctic shallow marine gas hydrate reservoir is insensitive to momentary
697 ocean warming. Nature Communications. https://doi.org/10.1038/ncomms15745.

Hong, W.-L., Torres, M.E., Portnov, A., Waage, M., Haley, B., Lepland, A., 2018. Variations in Gas and Water Pulses at an Arctic Seep: Fluid Sources and Methane Transport. Geophysical Research Letters 45 https://doi.org/10.1029/2018GL077309.

Hong, W.-L., Lepland, A., Himmler, T., Kim, J.-H., Chand, S., Sahy, D., D., Solomon, E., Rae, J., Tonu, M., Nam, S.-I., and Knies, J., 2019. Discharge of meteoric water in the eastern Norwegian Sea since the last glacial period. Geophysical Research Letters, 46. https://doi.org/10.1029/2019GL084237.

Hustoft, S., Bünz, S., Mienert, J., Chand, S., 2009. Gas hydrate reservoir and active methane-venting province in sediments on < 20 Ma young oceanic crust in the Fram Strait, offshore NW-Svalbard. Earth and Planetary Science Letters 284, 12-24. http://dx.doi.org/10.1016/j.epsl.2009.03.038.

Ijiri, A., Inagaki, F., Kubo, Y., Adhikari, R.R., SHattori, S., Hoshino, T., Imachi, H., Kawagucci, S., Morono, Y., Ohtomo, Y., Ono, S., Sakai, S., Takai, K., Toki, T., Wang, D.T., Yoshinaga, M.Y., Arnold, G.L., Ashi, J., Case, D.H., Feseker, T., Hinrichs, K.-U., Ikegawa, Y., Ikehara, M., Kallmeyer, J., Kumagai, H., Lever, M.A., Morita, Nakamura, K.-I., Nakamura, Y., Nishizawa, M., Orphan, V.J., Røy, H., Schmidt, F., Tani, A., Tanikawa, W., Terada, T., Tomaru, H., Tsuji, T., Tsunogai, U., Yamaguchi Y.T., Yoshida, N., 2018. Deep-biosphere methane production stimulated by geofluids in the Nankai accretionary complex. Science Advances, 4(6), 1– 15. https:/doi.org/10.1126/sciadv.aao4631

IPCC, 2013. Climate Change 2013: The Physical Science Basis. Contribution of Working Group I to the Fifth Assessment Report of the Intergovernmental Panel on Climate Change. In T.F. Stocker and others [eds.], Cambridge Univ. Press.

Jakobsson, M., Spielhagen, R.F., Thiede, J., Andreasen, C., Hall, B., Ingólfsson, Ó., Kjær, K. H., Van Kolfschoten, T. , Krinner, G., Long, A., Lunkka, J.-P., Subetto, D., Svendsen, J.I., 2008. Foreword to the special issue: Arctic paleoclimate and its extremes (APEX), Polar Res., 27(2), 97-104, doi:10.1111/j.1751-8369.2008.00063.x.

James, R.H., Bousquet, P., Bussmann, I., Haeckel, M., Kipfer, R., Leifer, I., Niemann, H., Ostrovsky, I., Pizkozub, J., Rehder, G., Treude, T., Vielsdädte, L., Greinert, J., 2016. Effects of climate change on methane emissions from seafloor sediments in the Arctic Ocean: A review. Limnology and Oceanography 61, 283–299. doi: 10.1002/lno.10307

728 Kennett, J.P., Cannariato, K.G., Hendy, I.L., Behl, R.J., 2000. Carbon isotopic evidence for
729 methane hydrate instability during quaternary interstadials. Science 288, 128–133.

730 Kim, S.-T., O'Neil, J.R., Hillaire-Marcel, C. and Mucci, A., 2007. Oxygen isotope
731 fractionation between synthetic aragonite and water: Influence of temperature and Mg2+
732 concentration. Geochimica et Cosmochimica Acta 71, 4704-4715.

733 Kvenvolden, K.A. 1988. Methane hydrate—a major reservoir of carbon in the shallow
734 geosphere. Chemical Geology 71: 41–51. doi:10.1016/0009-2541(88)90104-0

735 Lea, D.W., Boyle, E.A., 1993. Determination of carbonate-bound barium in foraminifera and
736 corals by isotope dilution plasma-mass spectrometry. Chemical Geology 103, 73-84.

737 Loyd S.J., Sample, J., Tripati, R.E., Defliese, W.F., Brooks, K., Hovland, M., Torres, M.,
738 Marlow, J., Hancock, L.G., Martin, R., Lyons, T., Tripati, A.E., 2016. Methane seep
739 carbonates yield clumped isotope signatures out of equilibrium with formation temperatures.
740 Nature Communications 7:12274. DOI: 10.1038/ncomms12274.

741 Martin, R.A., Nesbitt, E.A., Campbell, K.A., 2007. Carbon stable isotopic composition of
742 benthic foraminifera from Pliocene cold methane seeps, Cascadia accretionary margin.
743 Paleogeography, Paleoclimatolgy, Paleoecology 246, 260-277.

744 Martin, R.A., Nesbitt, E.A., Campbell, K.A., 2010. The effects of anaerobic methane
745 oxidation on benthic foraminiferal assemblages and stable isotopes on the Hikurangi Margin
746 of eastern New Zealand. Marine Geology 272, 270–284. doi:10.1016/j.margeo.2009.03.024.

747 Maslin, M., Viela, C., Mikkelsen, N., Grootes, P., 2005. Causes of catastrophic sediment
748 failures of the Amazon Fan. Quaternary Science Reviews 24, 2180-2193.

749 McCorkle, D.C., Keigwin, L.D., Corliss, B.H., Emerson, S. R., 1990. The influence of
750 microhabitats on the carbon isotopic composition of deep-sea benthic foraminifera.
751 Paleoceanography 5, 161–185.

752 McGuire, A. D., Anderson, L.G., Christensen, T. R., Dallimore, S., Guo, L., Hayes, D.J.,
753 Heimann, M., Lorenson, T. D., MacDonald, R. W., Roulet, N., 2009. Sensitivity of the carbon
754 cycle in the Arctic to climate change, Ecol. Monogr., 79(4), 523-555, doi:10.1890/08-2025.1.

755 Murray, J.W., 2006. Ecology and applications of benthic foraminifera, Cambridge University
756 Press.

757 Naehr, T.H., Eichhubl, P., Orphan, V.J., Hovland, M., Paull, C.K., Ussler, W. III, Lorenson,
758 T.D., Green, H.G., 2007. Authigenic carbonate formation at hydrocarbon seeps in continental
759 margin sediments: a comparative study. Deep Sea Research Part II: Topical Studies in
760 Oceanography, 54, 1268-1291.

761 Naehr, T.H., Birgel, D., Bohrmann, G., MacDonald, I.R., Kasten, S., 2009. Chemical Geology
762 266, 390-402. Biogeochemical controls on authigenic carbonate formation at the Chapopote
763 "asphalt volcano", Bay of Campeche. https://doi.org/10.1016/j.chemgeo.2009.07.002.

764 O'Neil, J.R. and Epstein, S., 1966. Oxygen Isotope Fractionation in the System Dolomite-
765 Calcite-Carbon Dioxide. Science 152, 198-201. DOI: 10.1126/science.152.3719.198.

766 Orphan W.G., Ussler W. III, Naehr, T.H., House, C.H., Hinrichs, K.-U., Paull, C.K., 2004.
767 Geological, geochemical, and microbiological heterogeneity of the seafloor around methane
768 vents in the Eel River Basin, offshore California, Chemical geology 205, 265-289.

769 Panieri, G., 2006. Foraminiferal response to an active methane seep environment: A case
770 study from the Adriatic Sea. Marine Micropaleontology. 61, 116–130.
771 http://dx.doi.org/10.1016/j.marmicro.2006.05.008.

772 Panieri, G., Camerlenghi, A., Conti, S., Pini, G.A., Cacho, I., 2009. Methane seepages
773 recorded in benthic foraminifera from Miocene seep carbonates,Northern Apennines (Italy).
774 Palaeogeography, Palaeoclimatology, Palaeoecology 284, 271-282.

775 Panieri, G., Camerlenghi, A., Cacho, I., Sanchez Cervera, C., Canals, M., Lafuerza, S.,
776 Herrera, G., 2012. Tracing seafloor methane emissions with benthic foraminifera: Results
777 from the Anasubmarine landslide (Eivissa Channel, Western Mediterranean Sea). Marine
778 Geology 291-294, 97-112.
779
780 Panieri, G., James, R.H., Camerlenghi, A., Cesari, V., Cervera, C.S., Cacho, I., Westbrook,
781 G.K., 2014. Record of methane emissions from the West Svalbard continental margin during
782 the last 16,000 years revealed by $\delta^{13}C$ of benthic foraminifera. Global and Planetary Change
783 122, 151–160. http://dx.doi.org/10.1016/j.gloplacha.2014.08.014.

784 Panieri, G., Graves, C.A., James, R.H., 2016. Paleo-methane emissions recorded in
785 foraminifera near the landward limit of the gas hydrate stability zone off-shore western
786 Svalbard. Geochemistry, Geophysics, Geosystem 17 (2), 521–537.
787 http://dx.doi.org/10.1002/2015GC006153.

788 Panieri, G., Bünz, S., Fornari, D.J., Escartin, J., Serov. P., Jansson, P., Torres, M.E., Johnson,
789 J.E., Hong, W.L., Sauer, S., Garcia, R., Gracias, N., 2017a. An integrated view of the methane
790 system in the pockmarks at Vestnesa Ridge, 79°N. Marine Geology 390, 282-300.
791 http://dx.doi.org/10.1016/j.margeo.2017.06.006.

792 Panieri, G., Lepland, A., Whitehouse, M.J., Wirth, R., Raanes, M.P., James, R.H., Graves,
793 C.A., Crémière, A., Schneider, A., 2017b. Diagenetic Mg-calcite overgrowths on
794 foraminiferal tests in the vicinity of methane seeps. Earth and Planetary Science Letters 458,
795 203-212. http://dx.doi.org/10.1016/j.epsl.2016.10.024.

796 Petersen, C.J., Bünz, S., Hustoft, S., Mienert, J., Klaeschen, D., 2010. High-resolution P-
797 Cable 3D seismic imaging of gas chimney structures in gas hydrated sediments of an Arctic
798 sediment drift. Marine Petroleum Geology 27, 1981–1994.
799 http://dx.doi.org/10.1016/j.marpetgeo.2010.06.006.

800 Pierre, C., Rouchy, J.-M., Blanc-Valleron, M.M., 2002. Gas hydrate dissociation in the Lorca
801 Basin (SE Spain) during the Mediterranean Messinian salinity crisis. Sedimentary Geology
802 147, 247-252. https://doi.org/10.1016/S0037-0738(01)00232-9.

803 Racine, C., Bonnin, J., Nam, S.-I., Giraudeau, J., Biguenet, M., Dessandier, P.-A., Kim, J.-H.,
804 2018. Distribution of living benthic foraminifera in the northern Chukchi Sea. Arktos 4: 28.
805 https://doi.org/10.1007/s41063-018-0062-y

806 Rasmussen, T.L., Thomsen, E., Slubowska, M.A., Jessen, S., Solheim, A., Koc, N., 2007.
807 Paleoceanographic evolution of the SW Svalbard margin (76°N) since 20,000 ^{14}C yr BP.
808 Quaternary Research 67, 100–114.

809 Rathburn, A.E., Perez, E.M., Martin, J.B., Day, S.A., Mahn, C., Gieskes, J., Ziebis, W.,
810 Williams, D., Bahls, A., 2003. Relationships between the distribution and stable isotopic
811 composition of living benthic foraminifera and cold methane seep biogeochemistry in
812 Monterey Bay, California. Geochemistry, Geophysics, Geosystem 4.
813 http://dx.doi.org/10.1029/2003GC000595.

814 Ravelo, A. C., and Hillaire Marcel, C., 1999. The Use of Oxygen and Carbon Isotopes of
815 Foraminifera in Paleoceanography. In Proxies in Late Cenozoic Paleoceanography.
816 Developments in Marine Geology 1, 735-760.

817 Rise, L., Bøe, R., Riis, F., Bellec, V.K., Laberg, J.S., Eidvin, T., Elvenes, S., and Thorsnes,
818 T., 2013. The Lofoten-Vesterålen continental margin, North Norway: canyons and mass-
819 movement activity, Marine and Petroleum Geology, 45, 134-149.

820 Roberts, H.H. and Aharon, P., 1994. Hydrocarbon-derived carbonate buildups of the northern
821 Gulf of Mexico continental slope: A review of submersible investigations. Geo-Marine
822 Letters 14, 135-148.

823 Sauer, S., Hong, W.-L., Knies, J., Lepland, A., Forwick, M., Klug, M., Eichinger, F.,
824 Baranwal, S., Crémière, A., Chand, S. and Schubert, C.J. (2016) Sources and turnover of
825 organic carbon and methane in fjord and shelf sediments off northern Norway. Geochemistry,
826 Geophysics, Geosystems 17, 4011-4031.

827 Sauer, S., Crémière, A., Knies, J., Lepland, A., Sahy, D., Martma, T., Noble, S.R.,
828 Schönenberger, J., Klug, M. and Schubert, C.J., 2017. U-Th chronology and formation
829 controls of methane-derived authigenic carbonates from the Hola trough seep area, northern
830 Norway. Chemical Geology 470, 164-179.

831 Schönfeld, J., Alve, E., Geslin, E., Jorissen, F., Korsun, S., Spezzaferri, S., 2012. The
832 FOBIMO (FOraminiferal BIo-MOnitoring) initiative—Towards a standardized protocol for
833 soft-bottom benthic foraminiferal monitoring studies. Marine Micropaleontology 94-95, 1-13.

834 Schneider, A., Crémière, A., Panieri, G., Lepland, A., Knies, J., 2017. Diagenetic alteration of
835 benthic foraminifera from a methane seep site on Vestnesa Ridge (NW Svalbard). Deep-Sea
836 Research I 123, 22-34. http://dx.doi.org/10.1016/j.dsr.2017.03.001.

837 Schneider, A., Panieri, G., Lepland, A., Consolaro, C., Crèmiére, A., Forwick, M., Johnson,
838 J.E., Plaza-Faverola, A., Sauer, S., Knies, J., 2018. Diagenetically altered benthic foraminifera
839 reveal paleo-methane seepage. Quaternary Science Reviews 193, 98-117.

840 Schroeder, J.O., Murray, R.W., Leinen, M., Pflaum, R.C., Janecek, T.R., 1997. Barium in
841 equatorial Pacific carbonate sediment: Terrigenous, oxide, and biogenic association.
842 Paleoceanography 12, 125-146.

Schumacher, S., Jorissen, F., Mackensen, A., Gooday, A.I., Pays, O., 2010. Ontogenetic effects on stable carbon and oxygen isotopes in tests of live (Rose Bengal stained) benthic foraminifera from the Pakistan continental margin. Marine Micropaleontology 76, 92-103.

Screen, J.A., and Simmonds, I., 2010. The central role of diminishing sea ice in recent Arctic temperature amplification. Nature 464, 1334-1337.

Sen, A., Himmler, T., Hong, W.-L., Chitkara, C., Lee, R.W., Ferré, B., Lepland, A., Knies, J., 2019. Atypical biological features of a new cold seep site on the Lofoten-Vesterålen continental margin (northern Norway). Scientific Reports 9: 1762. https://doi.org/10.1038/s41598-018-38070-9

Sen Gupta, B.K., Aharon, P., 1994. Benthic foraminifera of bathyal hydrocarbon vents of the Gulf of Mexico: initial report on communities and stable isotopes. Geo-Marine Letters 14, 88–96.

Serov, P., Vadakkepuliyambattaa, S., Mienert, J., Patton, H., Portnov, A., Silyakova, A., Panieri, G., Carroll, M.L., Carroll, J., Andreassen, K., Hubbard, A., 2017. Postglacial response of Arctic Ocean gas hydrates to climatic amelioration. Proceedings of the National Academy of Sciences of the United States of America 114, 6215-6220.

Serreze, M.C. and Barry, R.G., 2011. Processes and impacts of Arctic amplification: A research synthesis. Global and Planetary Change 77, 85-96.

Sloan, E.D. Jr., Koh, C., 2007. Clathrate hydrates of natural gases, 3rd ed. CRC Press.

Spero, H.J., Bijma, J., Lea, D.W., Bemis, B. E., 1997. Effect of seawater carbonate concentration on foraminiferal carbon and oxygen isotopes. Nature 390, 497-500.

Steinle, L., Graves, C.A., Treude, T., Ferre, B., Biastoch, A., Bussmann, I., Berndt, C., Krastel, S., James, R.H., Behrens, E., Böning, C.W., Greinert, J., Sapart, C.-J., Schreinert, M., Sommer, S., Lehmann, M.F., Niemann, H., 2015. Water column methanotrophy controlled by a rapid oceanographic switch. Nature Geoscience 8, 378–382.

Tagliabue, A., Bopp., L., 2008. Towards understanding global variability in ocean carbon-13. Gloobal Biogeochemical Cycles 22, GB1025. doi:10.1029/2007GB003037.

870 Talwani, M. and Eldholm, O., 1977, Evolution of the Norwegian-Greenland Sea: Geological
871 Society of America Bulletin 88, 969–999. doi: 10.1130 /0016-606(1977)88<969:EOTNS>2.0
872 .CO;2.

873 Tarutani, T., Clayton, R.N., Mayeda, T.K., 1969. The effect of polymorphism and magnesium
874 substitution on oxygen isotope fractionation between calcium carbonate and water.
875 Geochimica et Cosmochimica Acta 33, 987-996. https://doi.org/10.1016/0016-
876 7037(69)90108-2.

877 Thatcher, K.E., Westbrook, G.K., Sarkar, S., Minshull, T.A., 2013. Methane release from
878 warming-induced hydrate dissociation in the West Svalbard continental margin: Timing,
879 rates, and geological controls. Journal of Geophysical Research: Solid Earth 118, 22-38.

880 Thiede, J., Winkler, A., Wolf-Welling, T., Eldholm, O., Myhre, A.M., Baumann, K.H.,
881 Henrich, R., Stein, R., 1998. Late Cenozoic history of the Polar North Atlantic: results from
882 ocean drilling. Quaternary Science Reviews 17, 185–208.

883 Thomas, D.J., Zachos, J.C., Bralower, T.J., Thomas, E., Bohaty, S., 2002. Warming the fuel
884 for the fire: Evidence for the thermal dissociation of methane hydrate during the Paleocene-
885 Eocene thermal maximum. Geology 30, 1067-1070.

886 Tomaru, H., Torres, M.E., Matsumoto, R., and Borowski, W.S., 2006. Effect of massive gas
887 hydrate formation on the water isotopic fractionation of the gas hydrate system at Hydrate
888 Ridge, Cascadia margin, offshore Oregon. Geochemistry Geophysics Geosystems, 7,
889 Q1000110.1029/2005gc001207,.

890 Torres, M.E., Mix, A.C., Kinports, K., Haley, B., Klinkhammer, G. P, McManus, J., de
891 Angelis, M. A., 2003. Is methane venting at the seafloor recorded by δ13C of benthic
892 foraminifera shells? Paleoceanography, 18 (3), 1062, doi:10.1029/2002PA000824.

893 Torres, M. E., Mix, A. C., and Rugh, W. D., 2005. Precise delta C-13 analysis of dissolved
894 inorganic carbon in natural waters using automated headspace sampling and continuous-flow
895 mass spectrometry. Limnology and Oceanography-Methods 3, 349-360.

896 Ussler, W., Paull, C.K., 2008. Rates of anaerobic oxidation of methane and authigenic
897 carbonate mineralization in methane-rich deep-sea sediments inferred from models and
898 geochemical profiles. Earth and Planetary Science Letters 266, 271-287.

899 Vasconcelos, C., McKenzie, J.A., Warthmann, R. and Bernasconi, S.M., 2005. Calibration of
900 the $\delta^{18}O$ paleothermometer for dolomite precipitated in microbial cultures and natural
901 environments. Geology 33.

902 Vogt, P.R., Crane, K., Sundvor, E., Max, M.D., Pfirman, S.L., 1994. Methane-generated (?)
903 pockmarks on young, thickly sedimented oceanic crust in the Arctic: Vestnesa Ridge, Fram
904 Strait. Geology 22, 255-258.

905 Walton, W.R., 1952. Techniques for recognition of living foraminifera. In: Contribution of
906 the Cushman Foundation for Foraminiferal Research. 3. pp. 56–60.

907 Wan, S., Feng, D., Chen, F., Zhuang, C., Chen, D., 2018. Foraminifera from gas hydrate-
908 bearing sediments of the northeastern South China Sea: Proxy evaluation and application for
909 methane release activity. Journal of Asian Earth Sciences 168, 125-136.

910 Wefer, G., Heinze, P.-M., Berger, W.H., 1994. Clues to ancient methane release. Nature 369,
911 282.

912 Whiticar, M.J., 1999. Carbon and hydrogen isotope systematics of bacterial formation and
913 oxidation of methane. Chemical Geology 161, 291-314.

914 Yao, H., Hong, W.-L., Panieri, G., Sauer, S., Torres. M.E., F. Lehmann, M.F., Gründger, F.,
915 Niemann, H., 2019. Fracture-controlled fluid transport supports microbial methane-
916 oxidizing communities at the Vestnesa Ridge. Biogeosciences 16, 2221-2232.

917 Yoshinaga, M. Y., Holler, T., Goldhammer, T., Wegener, G., Pohlman, J. W., Brunner, B.,
918 Kuypers, M. M., Hinrichs, K.-U., and Elvert, M., 2014. Carbon isotope equilibration during
919 sulphate-limited anaerobic oxidation of methane, Nature Geoscience, 7, 190.

920

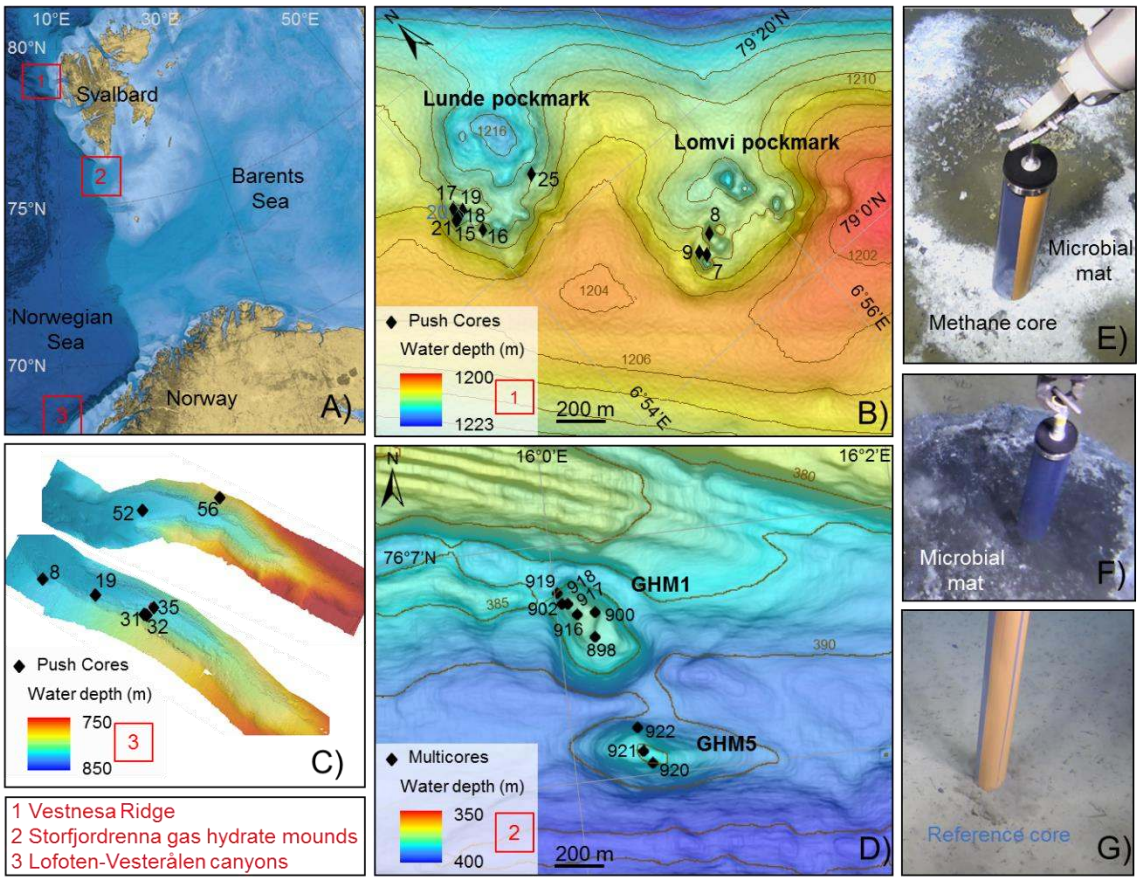

Figure 1. A) Map of the study area with sample areas identified by red squares. B) Location of the push cores collected within two pockmarks (Lunde and Lomvi) on Vestnesa Ridge. C) Location of push cores collected within the Lofoten-Vesterålen canyon region (Canyons North and South). D) Location of multicores collected in Storfjordrenna (GHMs 1 and 5). E) and F) Examples of push cores collected on microbial mats covering methane-rich sediments (i.e., cores V-8 and V-16, respectively) and G) Example of a push core collected outside a microbial mat (i.e., core V-20).

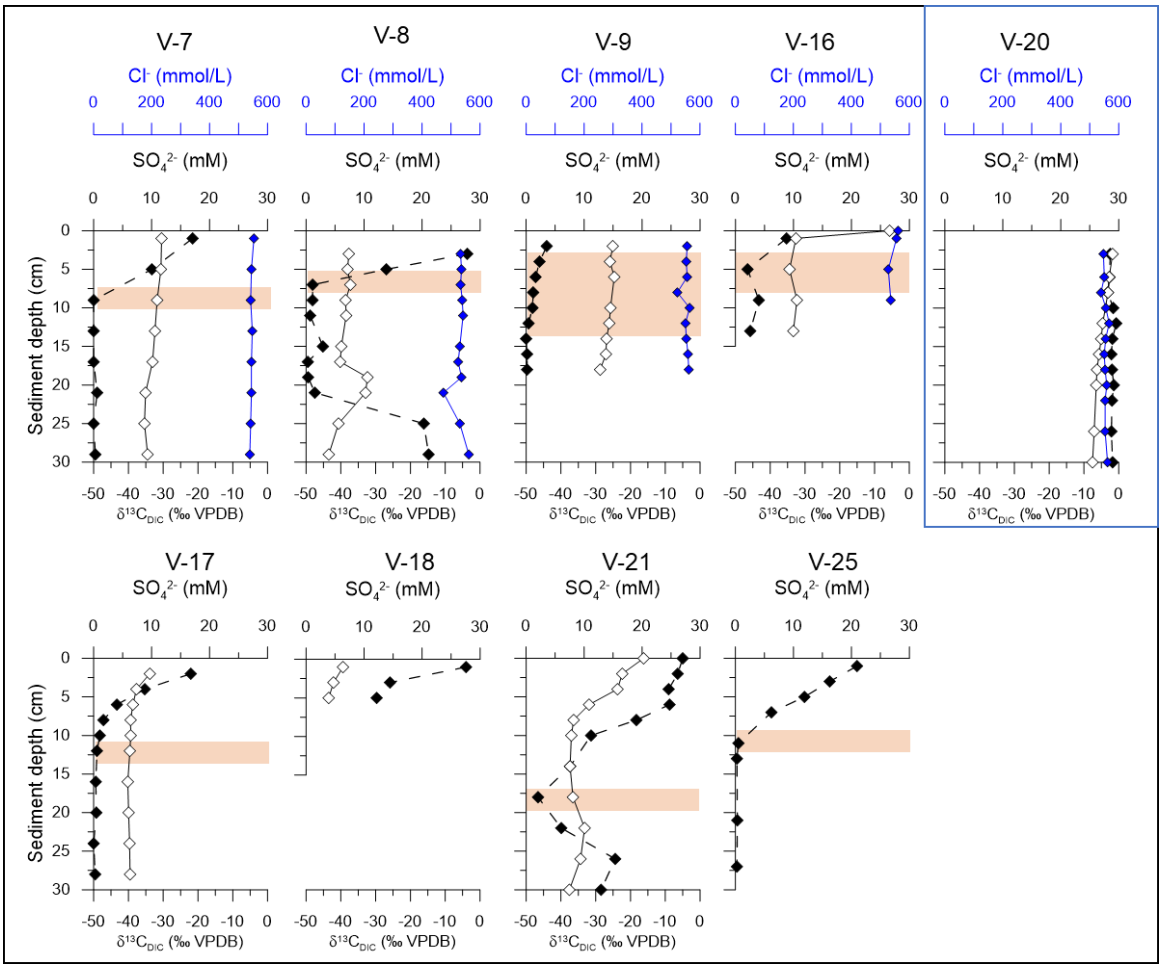

931

932 **Figure 2**. Pore water sulfate (SO_4^{2-}, black), $\delta^{13}C_{DIC}$ (white), and Chloride (Cl^-, blue) profiles
933 of push cores collected at Vestnesa Ridge. The numbers at the top of each graph identify the
934 stations; the blue square indicates the core sampled outside a microbial mat (control core).
935 The estimated sulfate-methane transition is in orange.

936

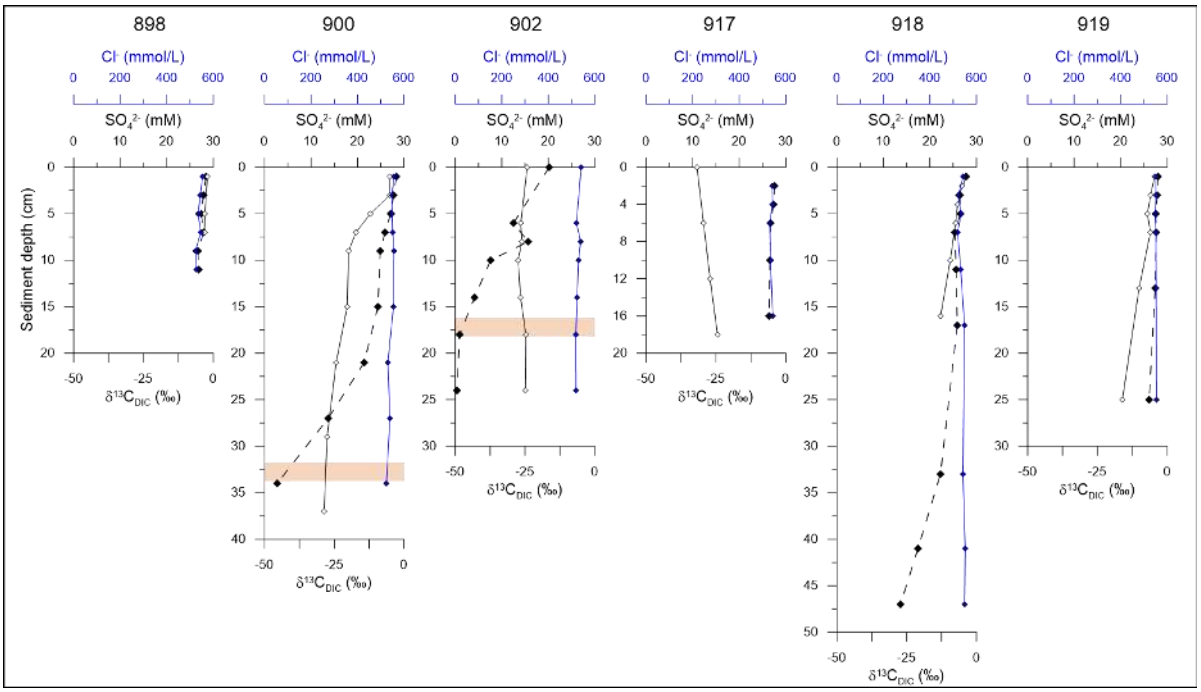

Figure 3. Pore water sulfate (SO_4^{2-}, black), $\delta^{13}C_{DIC}$ (white), and Chloride (Cl^-, blue) profiles of multicores collected at Storfjordrenna GHM1. The numbers at the top of each graph identify the stations; the estimated sulfate-methane transition is in orange.

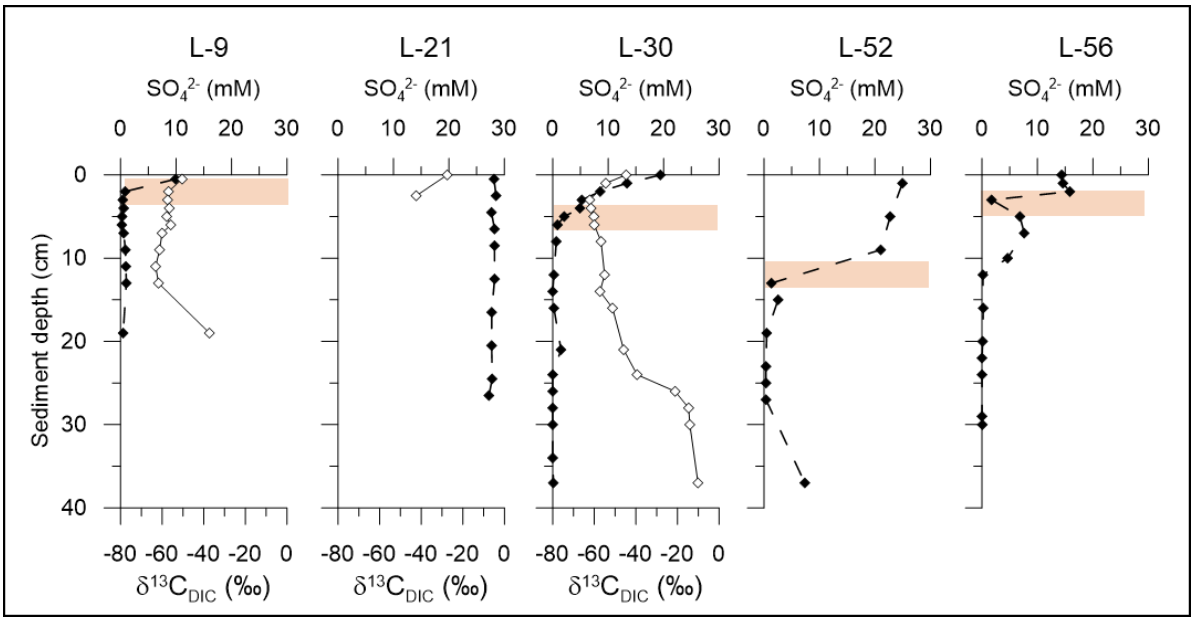

943
944

945 **Figure 4.** Pore water sulfate (SO_4^{2-}, black) and $\delta^{13}C_{DIC}$ (white) profiles of push cores
946 collected at the Lofoten-Vesterålen canyons. The numbers at the top of each graph identify
947 the stations; the estimated sulfate-methane transition is in orange.

948

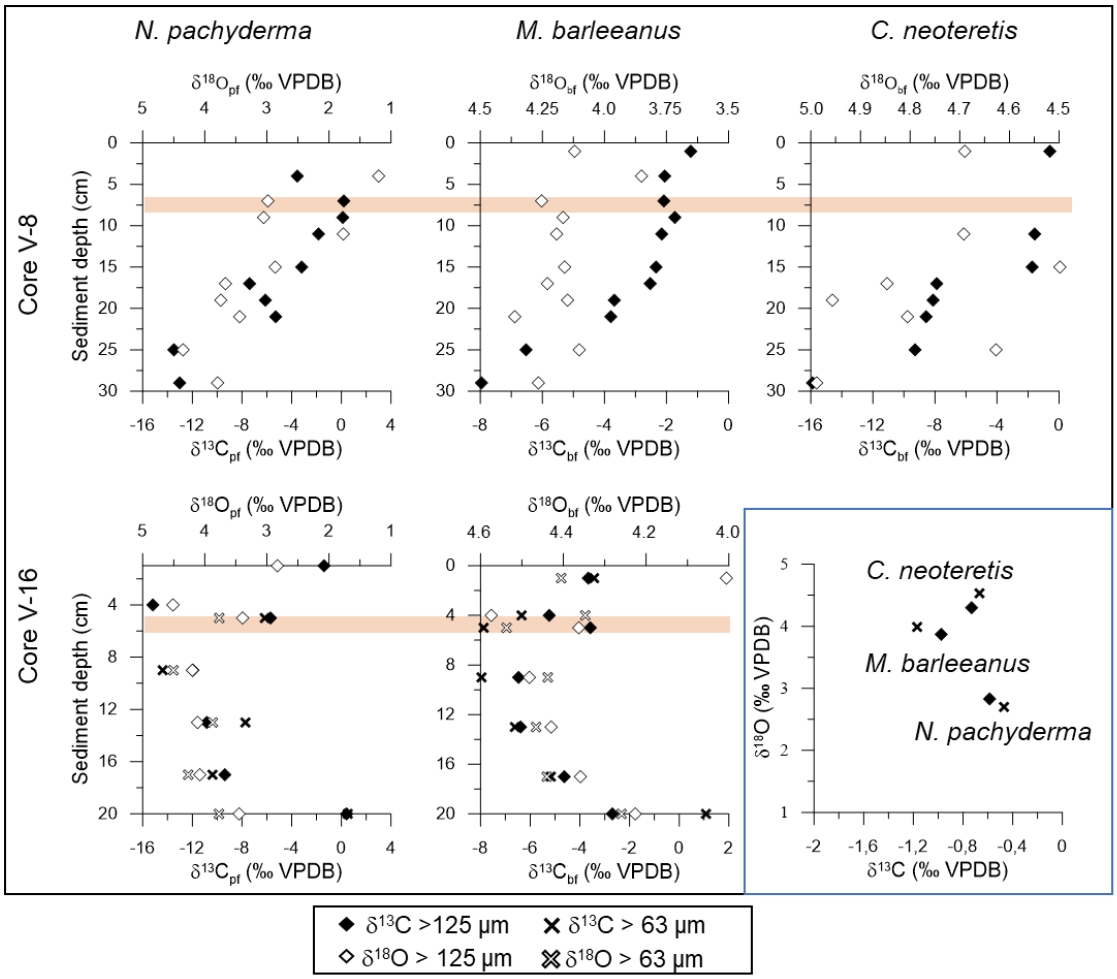

949

950 **Figure 5.** Cores V-8 and V-16 (Vestnesa Ridge) planktonic (pf) and benthic (bf) foraminiferal
951 isotopes ($\delta^{13}C$ and $\delta^{18}O$) data. The blue square indicates the values measured on the surface
952 sample (0-1 cm) of core V-20. Analyses were performed on two benthic (*C. neoteretis* and *M.*
953 *barleeanus*) and one planktonic (*N. pachyderma*) foraminiferal species. Diamonds are used to
954 identify data collected analyzing the fraction >125 µm. Crosses are used to identify data
955 collected analyzing the fraction >63 µm. VPDB = Vienna Pee Dee Belemnite.

956

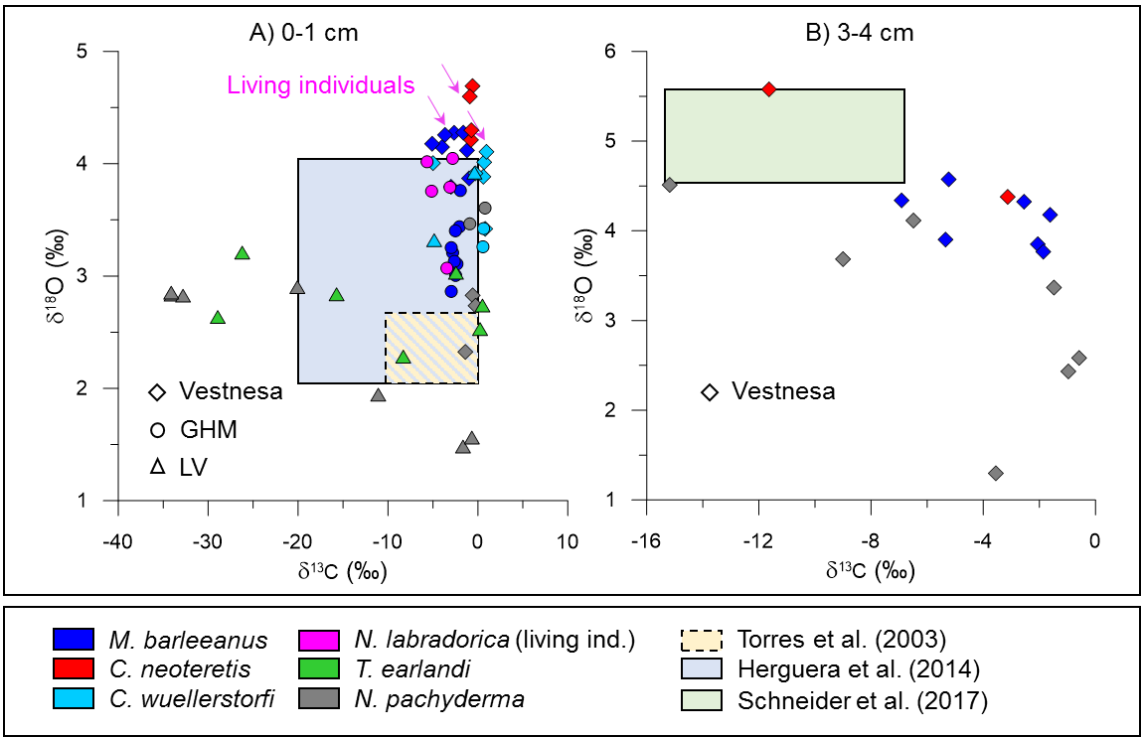

Figure 6. Foraminiferal stable isotopes ($\delta^{13}C$ and $\delta^{18}O$) measured on benthic (colored symbols) and planktonic (grey symbols) species. A) Data collected from surface samples (0-1 cm) of cores from Vestnesa Ridge, Storfjordrenna (GHM), and the Lofoten-Vesterålen Canyons. Data from Rose Bengal stained ('living') individuals are identified by pink arrows. B) Data collected from the interval 3-4 cm of cores collected at Vestnesa Ridge. Colored areas in (A) show the range of isotopic values of benthic foraminifera from methane seeps and gas hydrate-rich sediments from different geographic locations (Hydrate Ridge (in yellow) and Gulf of California (in blue); Torres et al., 2003, Herguera et al., 2014). All the foraminifera analyzed were picked from superficial sediments (0-5 cm) and were affected by secondary overgrowth. The green square in panel (B) shows the range of values measured on benthic foraminifera from Vestnesa Ridge (Schneider et al., 2017). The foraminifera analyzed were picked deeper in the sediment column (meters below the seafloor) and were affected by secondary overgrowth. VPDB = Vienna Pee Dee Belemnite.

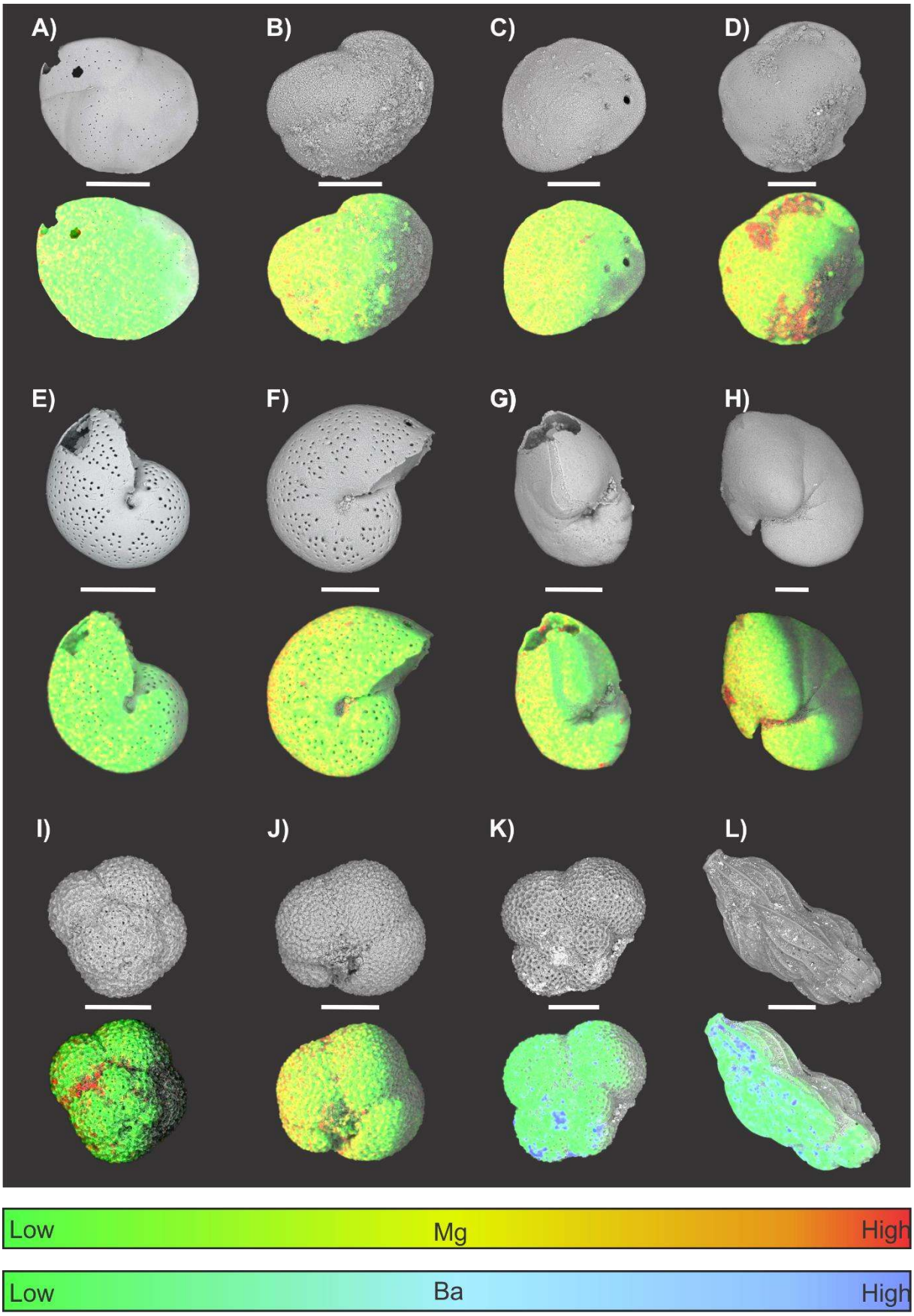

Figure 7. Backscatter-scanning electron microscopy images and corresponding energy-dispersive x-ray spectroscopy (EDS) maps of selected foraminiferal shells. *Cassidulina*

975 *neoteretis* from core V-16 0-1 cm (A) and 3-4 cm (B), and core V-8, 3-4 cm (C) and 29-30 cm
976 (D). *Melonis barleeanus* from core GHM1 0-1 cm (Rose Bengal stained specimen) (E), and
977 core V-8 29-30 cm (F). *Nonionella labradorica* from core GHM1 0-1 cm (Rose Bengal
978 stained specimen) (G), and core V-8 29-30 cm (H). *Neogloboquadrina pachyderma* from core
979 V-8 0-1 cm (I), core V-8 29-30 cm (J), and core L-8 0-1 cm (K). *Trifarina earlandi* from
980 Lofoten-Vesterålen L-19 0-1 cm (L). Scale bars are 100 µm. Grey areas on EDS maps
981 represent portions of the shells where the analysis was not possible, due to the angle of the
982 detector and shell morphology.
983
984

985 **Table 1.** Summary of the cores collected at Vestnesa Ridge (Lomvi and Lunde),
986 Storfjordrenna (GHMs 1 and 5), and the Lofoten-Vesterålen canyons (Canyons South and
987 North) and used in this study. The analyses performed on each core are specified. Chloride
988 data are not available for the LV Canyons cores. The data collected are reported in
989 Supplementary Tables 1, 2 and 3. Nd = no data.
990

Core reference	name	Location	latitude °N	longitude °E	water depth (m)	pore water SO_4^{2-}, $\delta^{13}C_{DIC}$, Cl^- (cm)	foraminifera stable isotopes (cm)
P1606-007	V-7	Lomvi	79.0023	6.225	1204	0-30	0-5
P1606-008	V-8	Lomvi	79.0027	6.9248	1208	0-30	0-30
P1606-009	V-9	Lomvi	79.0025	6.922	1205	0-20	0-5
P1606-015	V-15	Lunde	79.0076	6.9003	1208	0-30	0-2
P1606-016	V-16	Lunde	79.0068	6.9006	1206	0-15	0-20
P1606-017	V-17	Lunde	79.0078	6.8994	1205	0-30	0-5
P1606-018	V-18	Lunde	79.0075	6.899	1207	0-7	0-5
P1606-019	V-19	Lunde	79.0075	6.8986	1207	nd	0-5
P1606-020	V-20	Lunde	79.0075	6.899	1207	0-30	0-1
P1606-021	V-21	Lunde	79.0075	6.8989	1207	0-30	0-5
P1606-025	V-25	Lunde	79.0071	6.9111	1200	0-30	0-5
P1702-898	898	GHM1	76.1144	16.0033	380	0-12	0-1
P1702-900	900	GHM1	76.1150	16.0036	380	0-35	0-1
P1702-902	902	GHM1	76.1153	16.0011	377	0-25	0-1
P1702-916	916	GHM1	76.1150	16.0019	377	nd	0-1
P1702-917	917	GHM1	76.1153	16.0011	377	0-20	0-1
P1702-918	918	GHM1	76.1153	16.0006	389	0-50	0-1
P1702-919	919	GHM1	76.1156	16.0003	378	0-25	0-1
P1702-920	920	GHM5	76.1114	16.0075	379	nd	0-1
P1702-921	921	GHM5	76.1117	16.0067	380	nd	0-1
P1702-922	922	GHM5	76.1122	16.0064	386	nd	0-1
P1710-008	L-8	Canyon South	68.1583	10.4607	794	nd	0-1
P1710-009	L-9	Canyon South	68.1583	10.4606	794	0-20	nd
P1710-012	L-12	Canyon South	68.1591	10.4559	804	0-30	nd
P1710-019	L-19	Canyon South	68.1587	10.4561	794	nd	0-1
P1710-030	L-30	Canyon South	68.1578	10.4654	770	0-40	nd
P1710-031	L-31	Canyon South	68.1578	10.4653	769	nd	0-1
P1710-032	L-32	Canyon South	68.1578	10.4654	769	nd	0-1
P1710-035	L-35	Canyon South	68.158	10.4658	778	nd	0-1
P1710-052	L-52	Canyon North	68.1665	10.4633	807	0-40	0-1
P1710-056	L-56	Canyon North	68.1671	10.4702	782	0-30	0-1

991
992